Multiple-input Multiple-output Grating Lobe Selection Scheme for Radar Applications

Master thesis

Nick Cancrinus

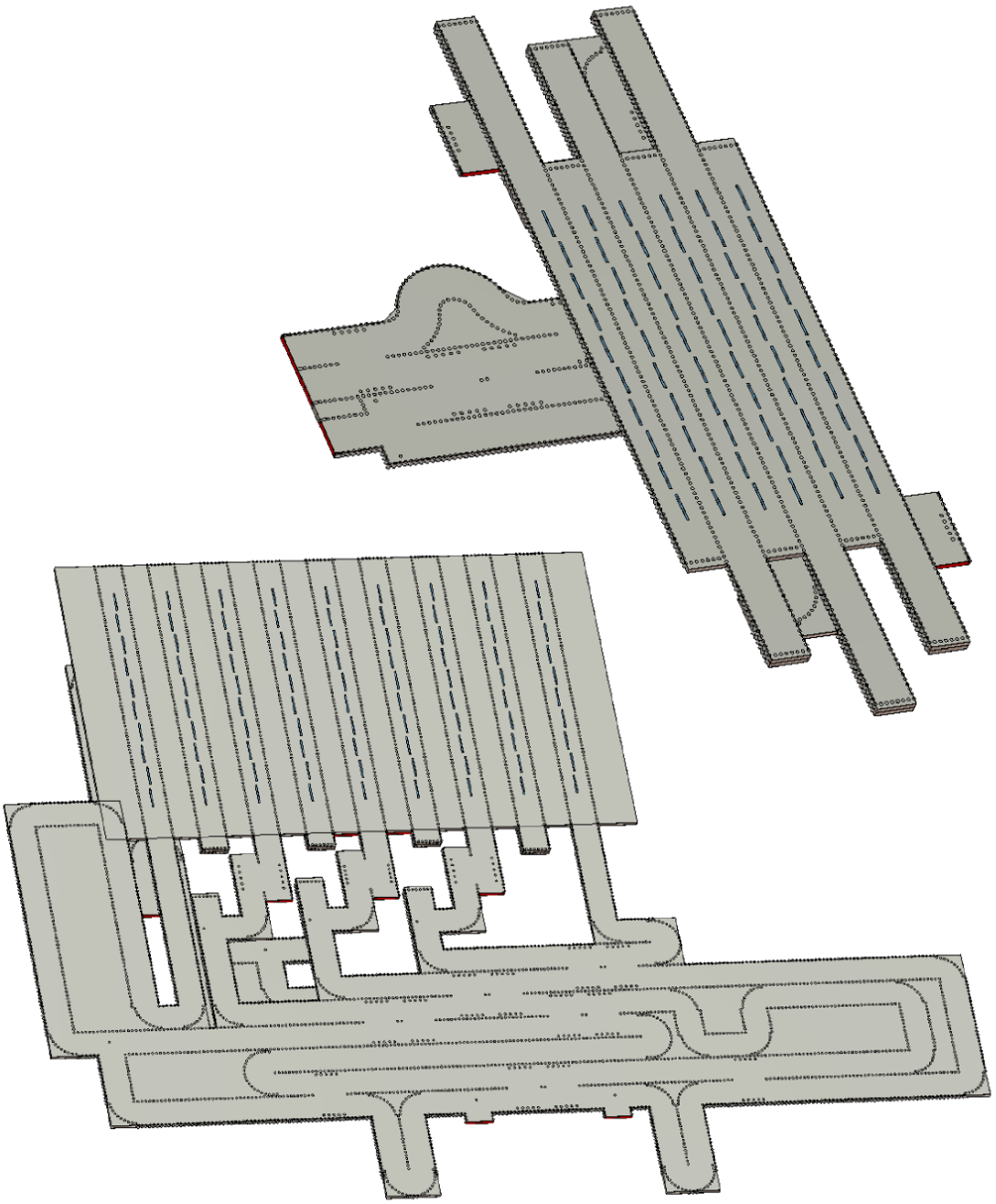

TU Delft

Multiple-input Multiple-output Grating Lobe Selection Scheme for Radar Applications

by

Nick Cancrinus

to obtain the degree of Master of Science
at the Delft University of Technology,
to be defended publicly on Monday August 26, 2019 at 11:00 AM.

Student number:	4377109	
Project duration:	November 12, 2018 – August 26, 2019	
Thesis committee:	Prof. dr. A. Yarovoy,	TU Delft, supervisor
	Prof. dr. C. Vaucher,	TU Delft
	Dr. O.A. Krasnov,	TU Delft
	Dr. J. Puskely,	TU Delft, daily supervisor

This thesis is confidential and cannot be made public until (to be determined).

An electronic version of this thesis is available at `http://repository.tudelft.nl/`.

TU Delft

Abstract

For radar applications, MIMO is often used. The problem is that the amount of available transmit- and receive channels is limited. If each channel is connected to a single antenna element, the effective aperture is small, and therefore the beamwidth is large and the angular resolution is limited. To circumvent this problem, a grating-lobe selection scheme is proposed. In this scheme, on the one hand, different transmit beams are used to select multiple grating lobes of the receive beam patterns. On the other hand, beamforming networks are used to connect every available digital channel to a single beam pattern. The result is an array that covers a reduced part of the visible space, with discrete beams that have improved beamwidth. The system gives the possibility to improve the angular resolution at the cost of field of view. A CST-model is made to verify this concept. In the specific example given in this thesis, the half-power beamwidth is improved from 8.4° at broadside, to 5.7° at broadside. At the same time the coverage is reduced from a theoretical ±90 degrees, to ±50 degrees.

Preface

This thesis was written as finalization of the Master Electrical Engineering at TU Delft. The project was done at the Microwave Sensing, Signals and Systems (MS3) group, which falls under the department Microelectronics. The field of the thesis is multiple-input multiple-output radar systems and the goal of the thesis is to implement a new design that can improve the performance in some aspects and can create more design freedom for these kind of radar systems.
I would like to thank my supervisor prof. dr. A. Yarovoy and my daily supervisor dr. J. Puskely for all their help. I would also like to thank prof. dr. C. Vaucher and dr. A. Roederer for their advice.

Nick Cancrinus
Delft, July 2019

Contents

1

Problem, goal and requirements

The goal of the first chapter is to give an introduction, and to state the problem and the goal. Next, the requirements for the designed system are given. Finally, an overview for the rest of the thesis is given. Section 1.1 gives the introduction and the problem definition. In section 1.2, the goal of the thesis is stated. In section 1.3, the design requirements are given. Finally, in section 1.4, an overview of the rest of the thesis given.

1.1. Introduction and problem definition

In this section first some background information is given on the area of the thesis, which is automotive radar. Next, some information is given on the state of the art of radar sensors. After this, the problem that this thesis tries to solve is described. Beforehand, it is noted that the design in this thesis was created with automotive radar in mind, different applications are also possible. Some examples could be 5G communications, indoor radar, internet of things or security. More generally, the design can be used for applications where beam scanning is desired.

First some background information is given on the area of the thesis, which is automotive radar. In recent years self-driving vehicles have become increasingly more important. Self-driving vehicles make it possible to improve road safety and traffic flow. They also remove the requirement for a human driver to be actively controlling the vehicle.
A sensor that is used in self-driving vehicles is automotive radar [1]. In this case antennas are placed on the exterior of the vehicle. One antenna is used to transmit an electromagnetic pulse into the space around the vehicle. This pulse will reflect from objects in the vicinity of the vehicle. Another antenna, or the same antenna, is used to receive the reflections. The time it takes for reflections to return and the frequency shift of the reflections can be used to obtain information on the range and speed of the reflecting objects.
Advantages of radar when compared with camera systems are as follows. Firstly, for radar it is not important whether it is day- or nighttime. Second, radar is more robust against changing wheather conditions. Another advantage is that range and speed information of reflecting objects is directly provided.

Often multiple-input multiple-output (MIMO) systems are used for automotive radar [2–4]. In this case one antenna array is used on the transmit-side (TX) and one on the receive-side (RX). The combination of these antenna arrays determines the effective beam pattern. The arrays are fed by digital chips. The amount of channels on these chips is limited. There could for example be 3 TX channels and 4 RX channels. If every channel is connected to a single antenna element, the effective aperture size is limited, which means that the directivity is limited. This is the main problem that this thesis tries to solve. More details will be given in chapter 2, section 2.1.

Before moving on to the next section, the following is noted. To increase the effective aperture of the antenna, it is possible to use a feeding structure that combines a larger amount of antenna elements into several uncoupled inputs. Every inputs synthesizes one radiation pattern. One example of such a feeding structure is the Butler matrix [5–9]. This is mentioned here, because these feeding structures will be used in the proposed solution to the problem.

1.2. Goal

In this section the main goal of the thesis will be described. First the problem definition given in the previous section will be repeated. The main problem is that often all available digital channels are coupled to a single antenna element. This means that the effective aperture is limited, which means that the directivity or angular resolution is limited.

Now the main concept that is used to solve this problem will be briefly introduced. Firstly, feeding networks will be used to couple every single digital channel to a single antenna beam pattern. This is important, but not the main aspect of the solution. More important is that the antenna beams are selected in such a way that full coverage of some limited angular area is obtained. This is done by choosing the transmit beams such that they can differentiate between different grating lobes of the receive beams. This means that any grating lobe of a receive beam can be used unambiguously, as long as the correct transmit beam is selected. This concept will be called the grating lobe selection scheme. More details will be given in later chapters, especially chapter 2.

Now the goal of the thesis will be explicitly stated:
Use a grating lobe selection scheme and feeding networks to improve the directivity of a MIMO radar-system, without increasing the amount of used digital channels.

1.3. Design requirements

The design requirements will now be given. These describe the conditions that the final design should fulfill. The requirements are selected such that their fulfillment matches a solution to the problem described in section 1.1. The requirements are divided between functional and non-functional requirements. The functional requirements are directly related to what the system should do. The non-functional requirements describe all other requirements. Within these categories a division is made in three different categories: Beam pattern, feeding network and additional. The category beam pattern gives requirements related to the array factor of the design. The array factor that is meant is that of the transmitter and receiver combined. The category feeding network describes the requirements related to the network that feeds the antenna subarrays. The category additional gives all requirements that fall outside of the beam pattern and feeding network categories.

A. Functional requirements

1. Beam pattern

A1a. The MIMO-system should have scanning capabilities in the azimuth direction.

A1b. The angular resolution in the azimuth direction should be better than for the standard implementation of MIMO. This is the most important requirement, and the motivation for this thesis. In practice this means that the half-power beamwidth (HPBW) in azimuth direction should be less than 8.4 - 9.5 degrees, depending on the sidelobe level (SLL). More details related to this requirement will be given in chapter 2.

A1c. The final beam pattern may not have any grating lobes. There cannot be any ambiguous angular information.

A1d. There cannot be large gaps between adjacent discrete beam scanning options. This requirement exists to make sure that there are no blind spots in the area of coverage. The beam crossing level can be at most 8 dB below the peak power level. More preferable would be 5 dB below the peak power level.

A1e. There should be coverage of the angular area between azimuth angle $\phi = -45^\circ$ and $\phi = 45^\circ$.

A1f. The SLL in the azimuth direction should be at least 15 dB lower than the peak power level, preferably even 20 dB lower.

A1g. The HPBW in the elevation direction should be less than 10 degrees.

A1h. The SLL in the elevation direction should be at least 15 dB lower than the peak power level, preferably even 20 dB lower.

2. Feeding network

A2a. Both the transmit and receive feeding network should provide suitable amplitude distributions to the antenna elements. This means that the amplitude coefficients should be such, that all possible resulting beam patterns fulfill the beam pattern requirements.

3. Additional

A3a. If the center frequency was 78 GHz, the bandwidth (BW) should be at least 3 GHz. This means that the BW ratio should be at least 3.9%. The system will be designed at a different center frequency, but this BW ratio should still be achieved.

B. Non-functional requirements

1. Beam pattern

B1a. The antenna spacing should be selected, such that the impact of mutual coupling is as small as possible. Scan attenuation may only occur at scan angles where the effective beam pattern has a large power. The effect should not occur at angles where the gain is relatively low. When scan attenuation does occur, the effect may not be dominant.

2. Feeding network

B2a. The inputs of the transmit feeding network should be well matched. The reflection coefficient should be less than -15 dB, preferably less than -20 dB.

B2b. There should be low coupling between the different inputs of the transmit feeding network. The cross S-parameters should be less than -15 dB, preferably less than -20 dB.

B2c. The receive array should be well matched, for the inherent beam patterns of the array. This means that when the received beam pattern exactly matches one of the beam patterns for which the receive array was designed, the power that is reflected from the array back into space should be low. This reflected power should be less than -15 dB, preferably -20 dB.

B2d. Provided that the manually introduced losses are not taken into account, the beam patterns that can be created by the receive feeding network should be orthogonal to each other. This ensures that when some received amplitude coefficients do not match a part of the feeding network, the reflection will not contaminate the other outputs. To quantify this, when the received beam pattern is orthogonal to the amplitude coefficients that correspond to one of the outputs, the power that goes to this output should be at least 15 dB lower than the total received power, preferably even 20 dB lower. More details on this requirement are given in chapter 2.

B2e. If the system would be designed at a center frequency of 78 GHz, then the losses are important. They should be kept as low as possible. An estimate is that the combined path losses of the transmit and receive array should be less than 6 dB. For this thesis, the design is done at 24.1 GHz. At this frequency the combined path losses should be less than approximately 2.5 dB. These two values require more or less similar compactness compared to the wavelength. This ensures that scaling to a higher frequency band is still possible.

B2f. The losses that are introduced manually, for the transmit and receive array combined, should be less than 3 dB. More information on why losses are manually introduced is given in chapter 2, section 2.5.

B2g. The design of both feeding networks should be compact, to minimize the required space. This also helps to achieve requirement B1a. This requirement is not quantified, but there should not be large unused spaces within the feeding structure.

3. Additional

B3a. The system should have the same amount of digital channels as the standard MIMO system that is used as reference. This means there are 3 transmit channels and 4 receive channels.

B3b. The system is implemented in substrate integrated waveguide (SIW). More information on SIW technology and SIW components is given in chapter 3.

B3c. The radiating elements are longitudinal slots in the top of the SIW lines.

B3d. The system is designed in the ISM-band from 24 GHz to 24.25 GHz. The center frequency is taken to be 24.1 GHz. To fulfill requirement A3a, the BW of the system should be even larger than this frequency band. The design should be such, that it can be scaled to different frequency bands without major changes.

B3e. The system should be scalable to some extent. The design in this thesis is just a proof of concept, however, this concept should also be beneficial in a system with more digital channels.

1.4. Thesis overview

In this section, an overview of the rest of the thesis will be given. Figure 1.1 shows a block schematic. Every block corresponds to a chapter of the thesis. The order of chapters more or less matches the flow of the design process. For every chapter a small description will be given.

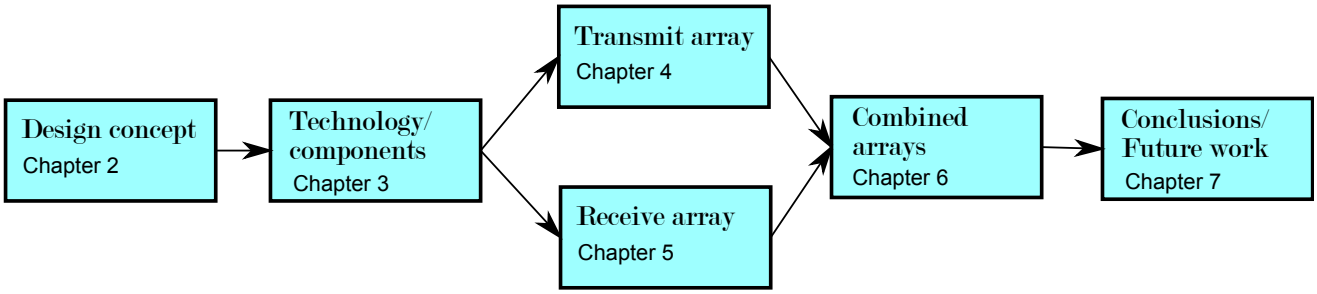

Figure 1.1: A block schematic that gives an overview of the thesis.

Chapter 2 gives the main concept that will be used to achieve improved angular resolution. First the problem will be defined in more detail. After this the main concept is explained. Next, the theoretical transmit and receive beam patterns are shown that can achieve improved angular resolution. The effect of mutual coupling between radiating elements is investigated. Finally, the orthogonality between different beam patterns is discussed.
Chapter 3 gives information about the used SIW technology and components that are used in the design. First some general information is given. Next, the SIW specifications for this project are given. Finally, the components used in this project are given.
Chapter 4 shows the design of the transmit array. First, the antenna beam coefficients are given. Next, a schematic overview of the implementation of the transmit array is given. After this a plot of the implementation is shown, that has the correct proportions. The CST-model of the TX array is shown. Finally, the simulation results are given.
Chapter 5 shows the design of the receive array. The lay-out of the chapter is the same as for chapter 4, about the transmit array. Some additional information is given about the orthogonality of the antenna beam coefficients, since this is more complex in the receive array.
Chapter 6 combines the simulation results of the simulations of the transmit and receive arrays, to obtain the simulated effective beam patterns. A comparison is done with the theoretical effective beam patterns. A discussion of the results is given.
Chapter 7 gives conclusions and possible future work.

2

Design concept

The main goal of this chapter is to give the main concept that will be used to achieve improved angular resolution. First the problem will be defined in more detail. After this the main concept is explained. Next, the theoretical transmit and receive beam patterns are shown that can achieve improved angular resolution. The effect of mutual coupling between radiating elements is investigated. Finally, the orthogonality between different beam patterns is discussed.

2.1. Detailed problem definition

In this thesis, a MIMO system with 3 transmit channels and 4 receive channels is considered. The common way to implement a system with this amount of channels is shown in figure 2.1. In this case the transmit channels are connected to antenna elements with a spacing of 0.5λ, such that there are no grating lobes in the transmit beam pattern. The receive channels are connected to antenna elements that are spaced further apart, in this case the spacing is 1.5λ. This means that the receive beam pattern has grating lobes. The transmit- and receive spacing are selected such, that when both arrays are combined, the transmit beam selects one of the grating lobes, and suppresses the others. An example of this is shown in figure 2.2. This method provides unambiguous angular information.

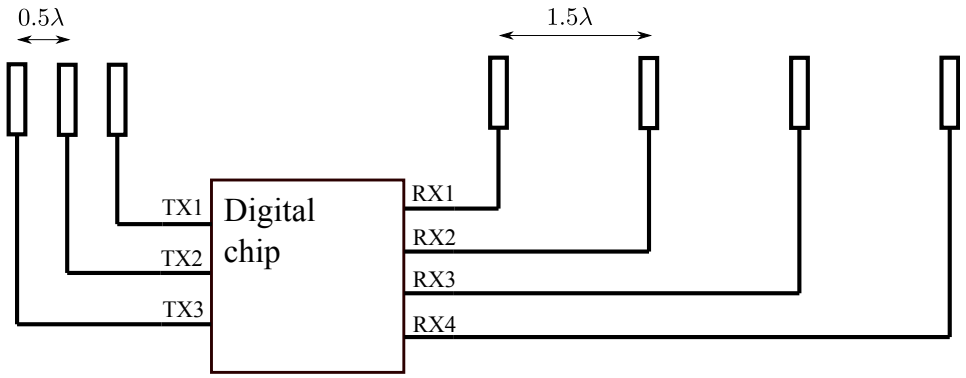

Figure 2.1: The common configuration for a MIMO system.

The main advantage of MIMO-radar as opposed to a regular phased array, is that the effective aperture, and therefore the angular resolution is increased to some extent. The MIMO-system also gives a full scan range of ±90 degrees, at least in theory. For the case of the MIMO-system with 3 TX channels and 4 RX channels, the -3 dB beamwidth is approximately 8.4 to 9.5 degrees, depending on the desired sidelobe level. Although this beamwidth is better than for the case of a phased array, it is still not very good. The reason for this is that when every channel is connected to a single antenna element, the maximum effective antenna aperture is limited. The goal of the thesis is to overcome this and to further improve the angular resolution.

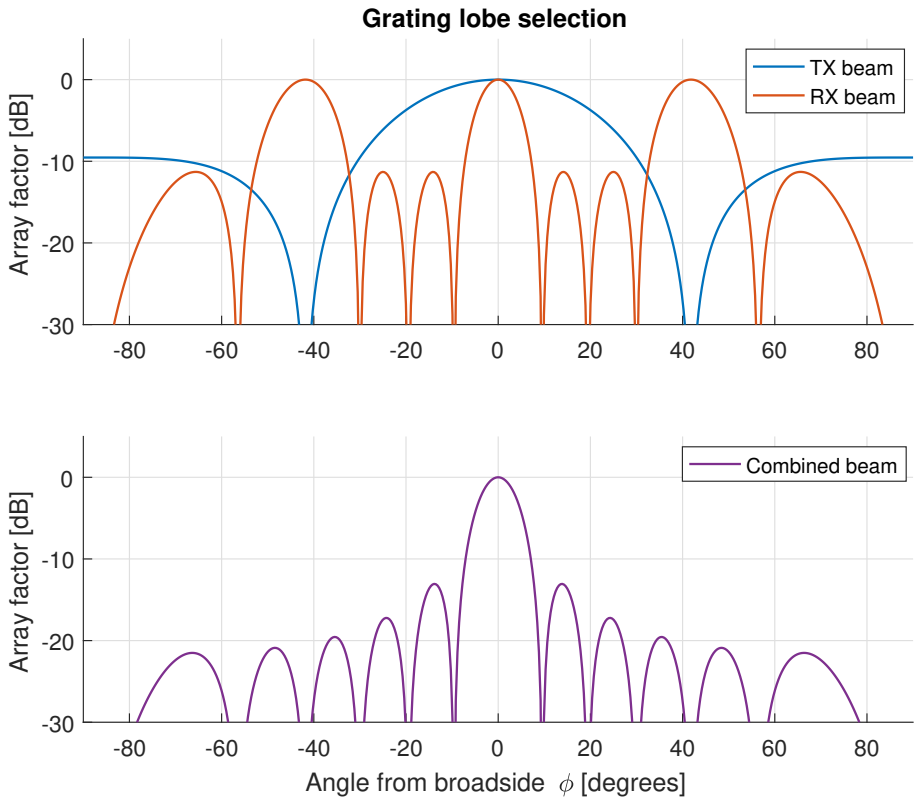

Figure 2.2: An example how one grating lobe is selected and the others are suppressed.

2.2. Design concept

The basis for the design proposal consists of two parts. The first part is as follows. In the current state of MIMO radar, one grating lobe of the receive beam pattern is selected and the other grating lobes are suppressed. Instead of doing this with only one grating lobe, it is also possible to actively do this for all grating lobes. In this case all grating lobes are used, instead of suppressing some. This makes it possible to obtain more information from a single beam pattern.

The second part is that to increase the effective aperture of the antenna, it is possible to use a beamforming network that combines a larger amount of antenna elements into several inputs. Every input synthesizes one radiation pattern. One example of such a feeding structure is the Butler matrix [5–9]. An alternative to the Butler matrix is the Rotman lens [10, 11]. When beamforming networks are used, all transmit and receive channels can be connected to beam patterns. This means that when one channel is activated, one beam pattern is activated.

When these two parts are combined, a system can be created that can place a few discrete transmit and receive beam patterns in such a way, that information from all grating lobes is used. This will be called the grating lobe selection scheme. When doing this, an important requirement is that full coverage of a certain angular area is maintained. There can be no blind spots. A system that is implemented in this way gives the opportunity to cover a decreased angular area with beams that have an improved directivity. This means that the angular resolution is improved. For example, in the specific implementation that will be given later, the coverage is ±50 degrees, but the -3 dB beamwidth is improved to 5.7 degrees.

The system is an expansion on the current state of the art that provides the possibility to improve the angular resolution at the cost of a decrease in angular coverage. The grating lobe selection scheme makes it possible to efficiently use the available amount of channels.

2.3. Theoretical implementation

In this section, a theoretical implementation of the explained concept will be given. The beamforming is assumed to be fully analog, which means that every channel is connected directly to a single beam pattern.

Table 2.1: Progressive phase shifts and amplitude coefficients for the different transmit channels. The coefficients are based on a Taylor window with maximum sidelobe level -25 dB.

	β	$\|t1\|$	$\|t2\|$	$\|t3\|$	$\|t4\|$	$\|t5\|$	$\|t6\|$
Channel 1	$-90°$	0.595	1.018	1.387	1.387	1.018	0.595
Channel 2	0	0.595	1.018	1.387	1.387	1.018	0.595
Channel 3	$90°$	0.595	1.018	1.387	1.387	1.018	0.595

This means that the phase capabilities of the digital MIMO-chip are not used, only the amplitudes of the channels are relevant. The reason for this is that in this case it was the most straightforward to design a proof of concept. In the design in this thesis, the transmit beam patterns are assumed to have no grating lobes, and the receive beam patterns are assumed to have grating lobes. In general, it is also possible to interchange this. Since there are 3 TX channels and 4 RX channels, there are 3 possible TX beams and 4 possible RX beams. The goal is to place these beams in such a way that the TX beams can select different RX grating lobes. It is also important that the beams provide full coverage of an angular area. Now, first the selection of the transmit beams will be shown. After this, the selection of the receive beams will be shown. Finally, the resulting effective beam patterns will be shown.

2.3.1. Transmit array

First, the selection of the transmit beams will be done. There are 3 TX channels, so there are 3 different TX beams. These beams do not have grating lobes. The goal is to place the transmit beams in such a way that full coverage of an angular area is obtained. To achieve this, it was chosen to have 6 antenna elements with a spacing of 0.5λ. This is shown in figure 2.3.

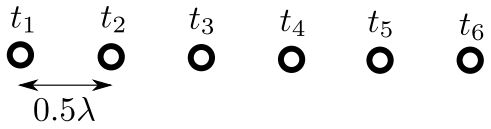

Figure 2.3: The antenna element positions of the transmit array.

The selected progressive phase shifts and amplitude coefficients for the three different beams are given in table 2.1. It can be seen that the progressive phase shifts are $-90°$,$0°$ and $90°$. This will simplify the design of the TX beamforming network. The amplitude coefficients are based on a Taylor window with maximum sidelobe level -25 dB.

Figure 2.4 shows the three corresponding transmit beam patterns. It can be seen that the coverage is approximately from $\phi = -45°$ to $\phi = 45°$, in line with requirement A1e. The power level in the gap between two beams is 6.4 dB below the peak power level, which makes sure requirement A1d can still be achieved. The sidelobe level of the three beams is 22.9 dB below the peak power level.

2.3.2. Receive array

Next, the selection of the receive beam patterns will be shown. There are 4 RX channels available, all of which are connected to a beam pattern via the beamforming network. The spacing of the array is chosen such that these beam patterns have grating lobes. The goal is to select these four beams in a way that the TX beams can correctly distinguish between different grating lobes. Full coverage of the desired angular area should be achieved.

For the receive array, it is chosen to have 9 antenna elements with a spacing of 1.0λ. This is shown in figure 2.5. Two of the beam patterns are connected to elements with this spacing of 1.0λ. The other two beam patterns are only connected to the odd elements, such that the effective spacing is 2.0λ. This is done to make sure that all grating lobes can be placed correctly with respect to the transmit beam.

Table 2.2 shows the progressive phase shifts and amplitude coefficients for the different receive channels. The selected progressive phase shifts are $-45°$, $45°$, $-90°$ and $90°$. These values are selected, because it simplifies the design of the feeding network. Furthermore, it can be seen that channel 1 and 2 are only connected to the odd antenna elements, such that the effective element spacing for these patterns is 2.0λ. Channel 3 and 4 are connected to antenna elements 2 up to 7, such that the element spacing for these patterns is 1.0λ. The amplitude coefficients are again based on a Taylor window. For channels 1 and 2, the maximum sidelobe

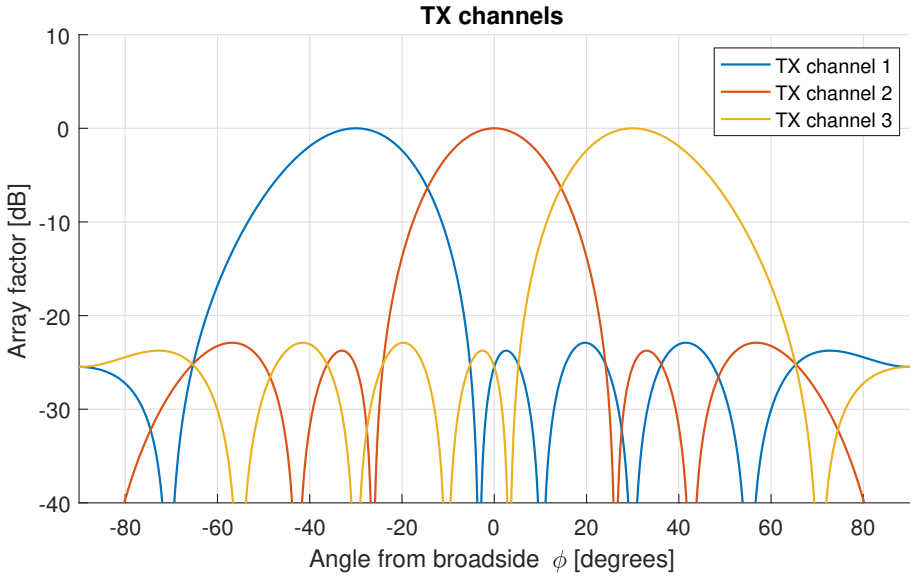

Figure 2.4: The transmit beam patterns.

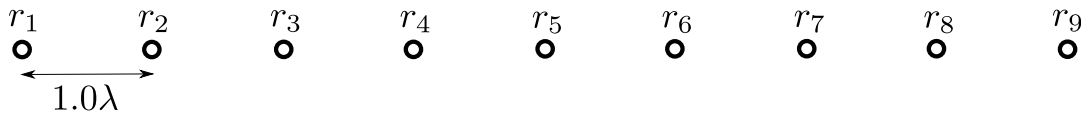

Figure 2.5: The antenna element positions of the receive array.

level of the Taylor window is -21 dB. For channels 3 and 4, the maximum sidelobe level of the Taylor window is -23.5 dB.

Figure 2.6 shows the beam patterns that correspond to channel 1 and 2. For these channels the effective spacing is 2.0λ, so the grating lobes are relatively close together. These two beams are placed such that every transmit beam covers one grating lobe, but does not overlap with another grating lobe. This means that when one transmit beam is activated, one grating lobe will be selected, and the others will be suppressed. The sidelobe level for these two beams is -18.7 dB with respect to the grating lobes.

Along with the beams for channel 1 and 2, figure 2.7 also shows the beam patterns that correspond to channel 3 and 4. For these two channels, the element spacing is 1.0λ, which means that the grating lobes are further apart. The grating lobes are placed such, that they fill the gaps left by the first two beam patterns. In this way full coverage is achieved. For channel 3 and 4 it still holds that all transmit beams select only one grating lobe. For these two beam patterns the sidelobe level is -21.8 dB.

2.3.3. Combined beam patterns

Now the effective beam patterns will be shown, that are obtained when the transmit- and receive arrays are combined. For a certain transmit channel and a certain receive channel, the effective beam pattern can be obtained by multiplying the transmit- and receive array factor. There are 3 transmit channels and 4 receive channels, so in total there are 12 combined beam patterns. Figure 2.8 shows all possible combined beam

Table 2.2: Progressive phase shifts and amplitude coefficients for the different receive channels. The amplitude coefficients are based on a Taylor window. For channels 1 and 2, the maximum sidelobe level of the Taylor window is -21 dB. For channels 3 and 4, the maximum sidelobe level of the Taylor window is -23.5 dB.

	β	$\|r1\|$	$\|r2\|$	$\|r3\|$	$\|r4\|$	$\|r5\|$	$\|r6\|$	$\|r7\|$	$\|r8\|$	$\|r9\|$
Channel 1	$-45°$	0.736	0	1.105	0	1.318	0	1.105	0	0.736
Channel 2	$45°$	0.736	0	1.105	0	1.318	0	1.105	0	0.736
Channel 3	$-90°$	0	0.627	0.911	1.266	1.393	1.266	0.911	0.627	0
Channel 4	$90°$	0	0.627	0.911	1.266	1.393	1.266	0.911	0.627	0

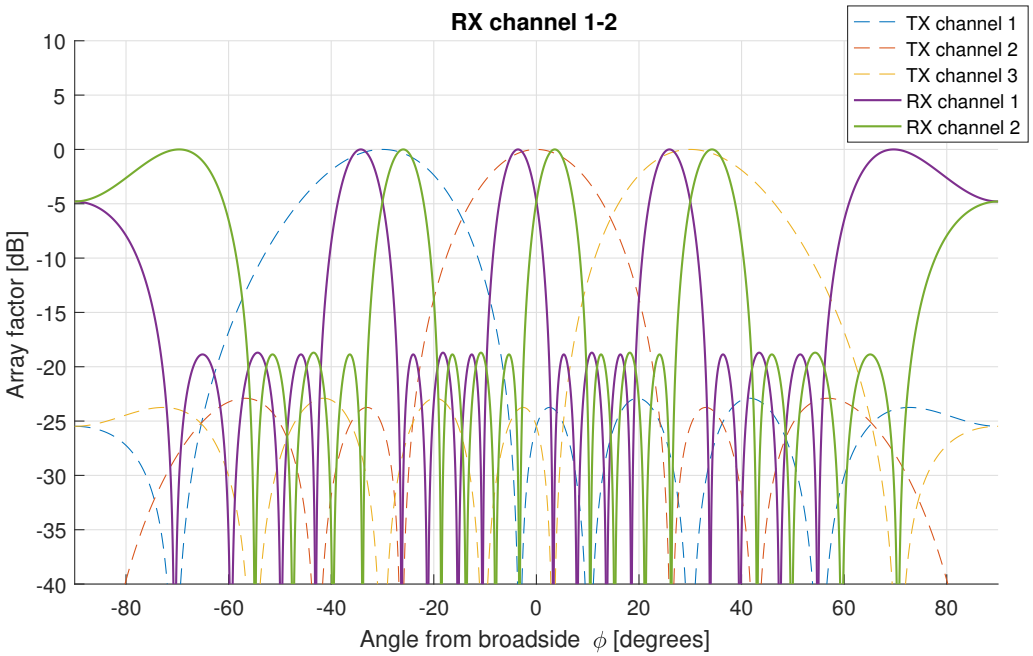

Figure 2.6: The receive beam patterns for RX channels 1 and 2.

patterns in one figure. It can be seen that there is good coverage from $\phi = -50°$ to $\phi = 50°$. The power level in the gaps between adjacent beam patterns is at most 7.1 dB lower than the peak power level.

Figure 2.9 shows all possible combined beam patterns, seperately. The level of the highest sidelobe differs between -17.5 dB and -19.3 dB for different beam patterns. For every beam pattern only a few sidelobes are at this level, many are much lower.

The most important improvement with respect to the common scenario given in section 2.1, is that the angular resolution has improved. For the common MIMO configuration, the effective aperture is 5.5λ. For this new configuration, the effective aperture is either 8.5λ or 10.5λ, depending on which beam is selected. When looking at the center beam, for the common MIMO configuration, the half power beamwidth was between 8.4 and 9.5 degrees, depending on the desired sidelobe level. For the new MIMO configuration, the HPBW of the beam near the center is 5.7 degrees.

To explain the function of the design in more detail, a use case will be given. For any radar measurement, first the TX beam is activated that corresponds to the direction of interest. After this, all the RX channels can be received simultaneously. The amplitudes of the four RX channels then correspond to reflections from the four corresponding beams in figure 2.8 or 2.9.

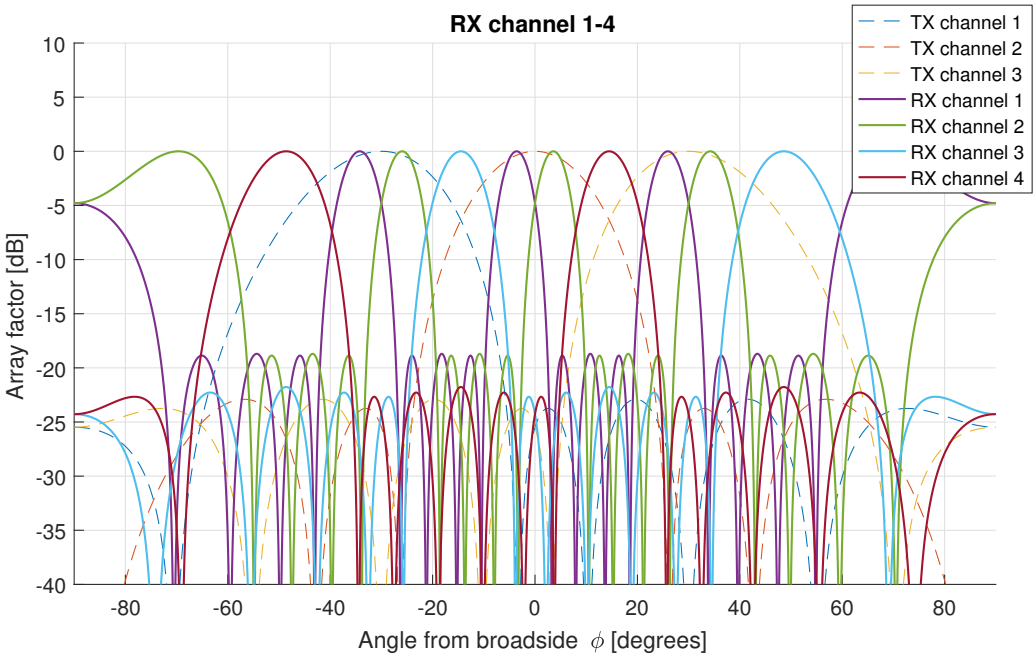

Figure 2.7: The receive beam patterns for all RX channels.

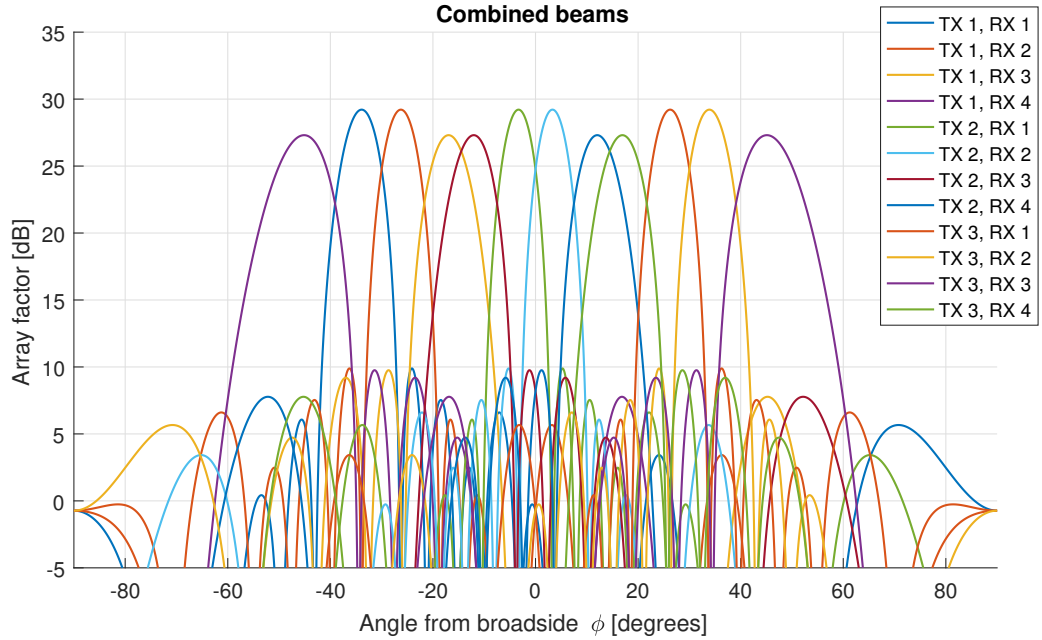

Figure 2.8: All possible combined beam patterns, in one figure.

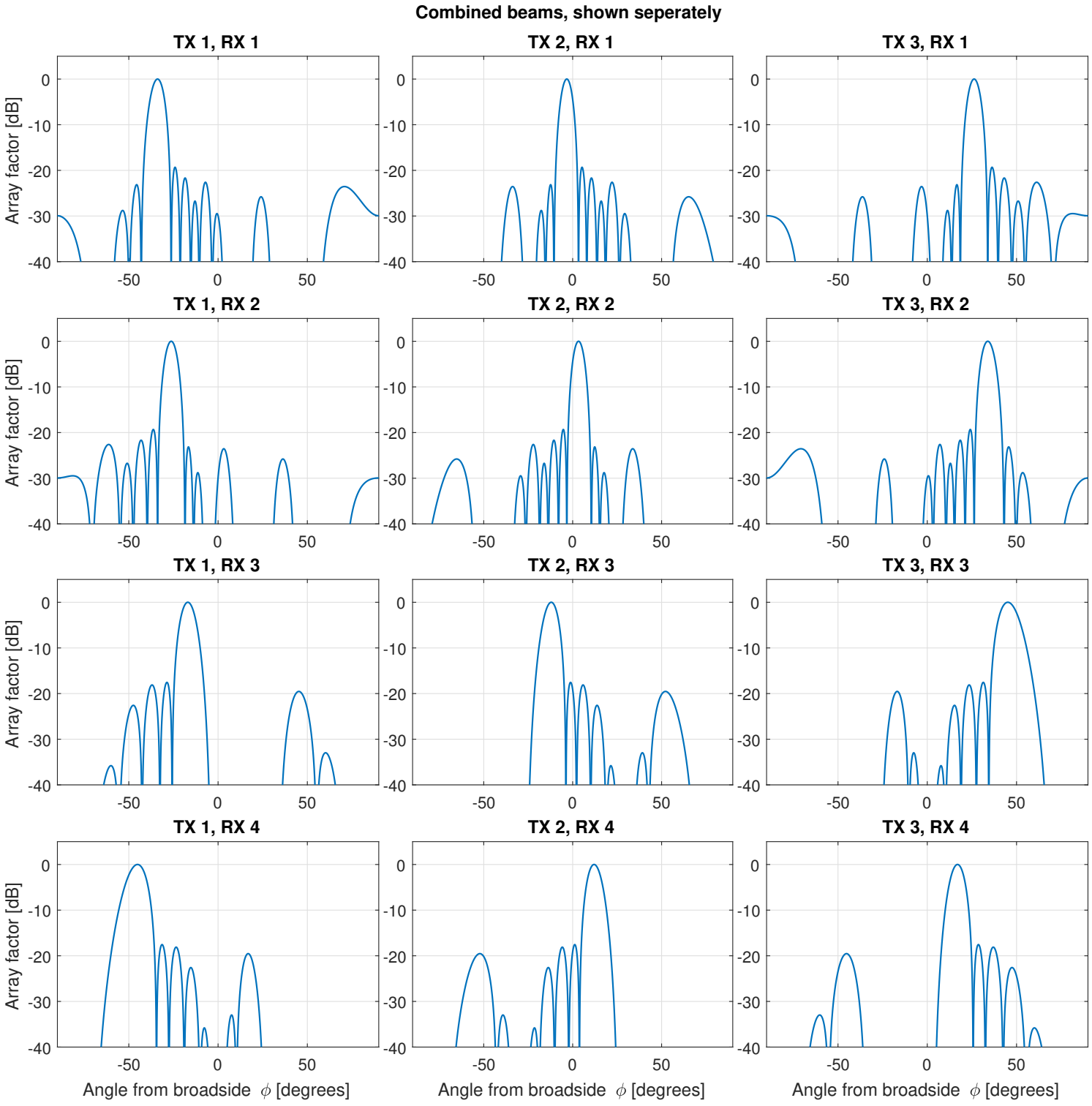

Figure 2.9: All possible combined beam patterns, shown seperately.

2.4. Mutual coupling

In this section, the effect of mutual coupling between antenna elements will be investigated. The radiating elements that are used are slots in a substrate integrated waveguide. In principle, slots can radiate towards every visible azimuth angle. For this reason the mutual coupling between antenna elements is important for this array design. The effect of mutual coupling can be described as follows. Information was obtained from [12–17]. The impact of mutual coupling is the largest at the scan angles where there is a grating lobe directed towards $\phi = -90^\circ$ or $\phi = 90^\circ$, along the array. In this case, signals coming from different antenna elements cause an impedance mismatch between the array and the feeding network. At these scan angles, attenuation of the transmitted power will occur. To quantify this effect, the method explained in [12] is used. In this case, first the embedded element pattern for every antenna element is obtained, via a simulation. For some scan angle, these can be combined into a total active array factor, that takes into account the scan attenuation. This can be repeated for a large amount of scan angles, to obtain a power envelope, that shows how large the attenuation is for these different angles. This analysis is only done for the receive array. The transmit array has fewer antenna elements, and the array spacing is smaller. Therefore, in this case, the mutual coupling is less important. Figure 2.10 shows the CST-model that is used to obtain the embedded element patterns. It can be seen that there are 9 elements on the azimuth axis, that provide the azimuth beam pattern. There are 10 elements on the elevation axis, that provide the elevation beam pattern. Dipoles are used instead of slots, because this simplifies the CST-model. This should have little effect on mutual coupling.

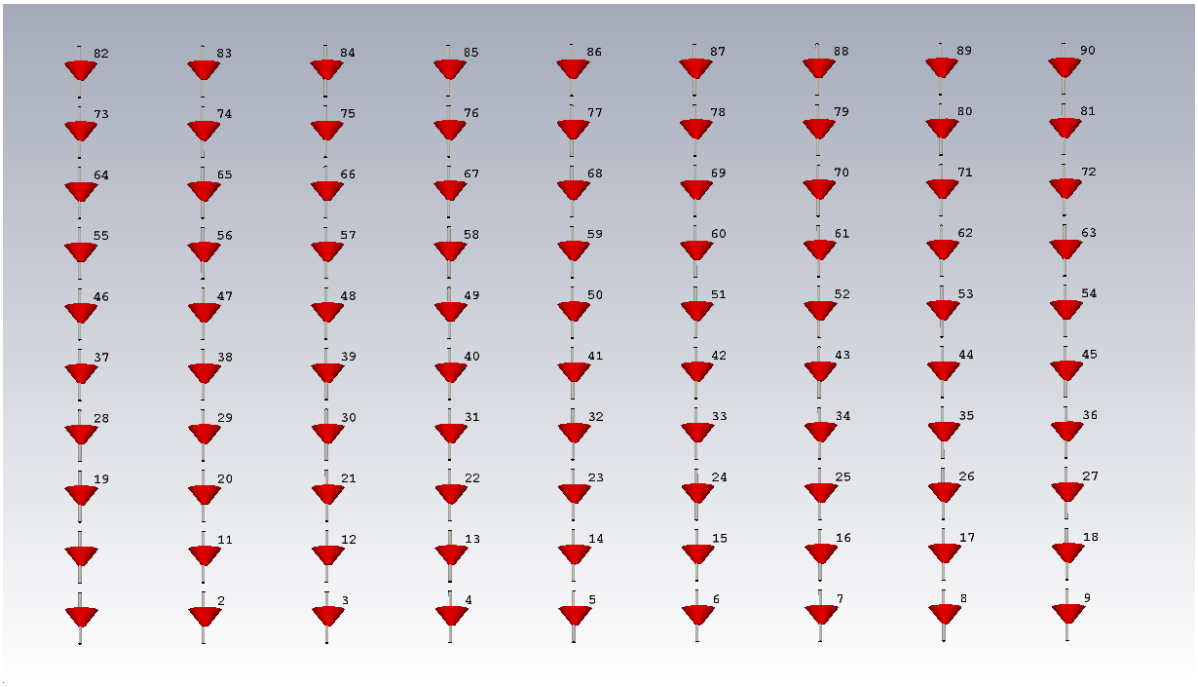

Figure 2.10: The CST model that is used to determine the effect of mutual coupling.

Figure 2.11 shows the normalized scan attenuation, due to mutual coupling. It can be seen that at the edges of the field of view, and at broadside, there is a drop in the gain. Since the element spacing is 1.0λ, these angles correspond with scan angles where a grating lobe enters the visible range. The gain drop at the center is 8.4 dB with respect to the angle with the least attenuation. The element spacing is selected, such that the gain drop falls at the peak power level of a transmit beam, and not in the gap between two beam patterns. For this reason, this level of mutual coupling was accepted.

2.5. Beam orthogonality

An additional requirement is that all transmit excitation coefficients and all receive excitation coefficients are orthogonal to eachother. Here the excitation coefficients are the amplitude and phase applied to different antenna elements. To define this orthogonality, suppose that $\mathbf{c_1}$ and $\mathbf{c_2}$ are two row vectors, that contain the excitation coefficients for two beam patterns. They are orthogonal when:

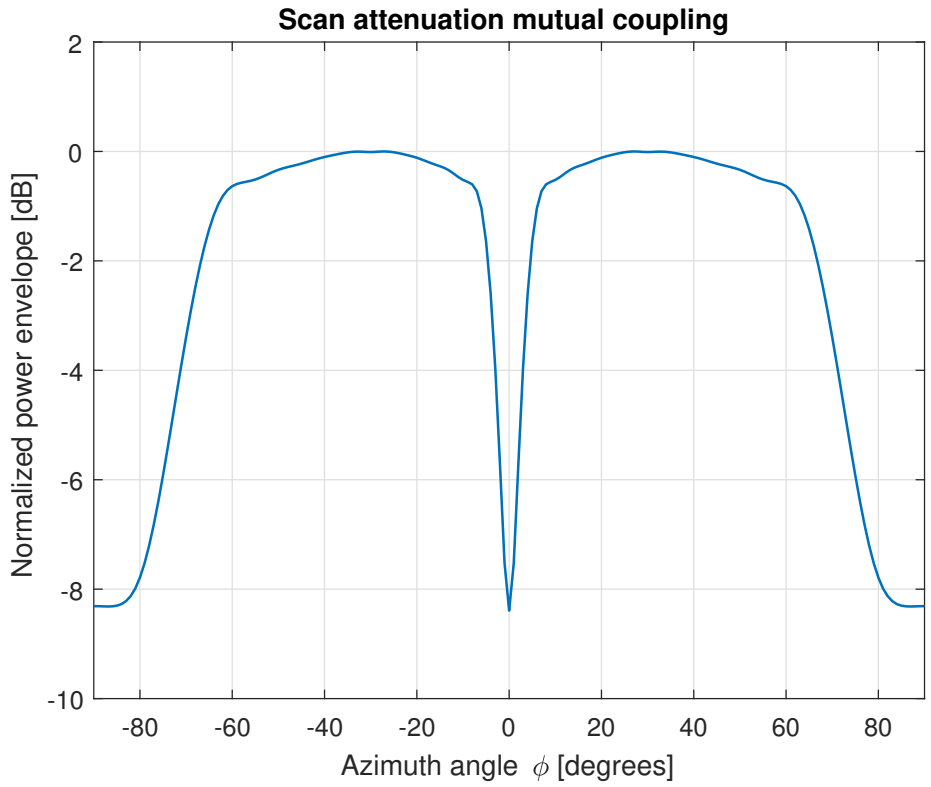

Figure 2.11: The scan attenuation at different angles due to mutual coupling.

$$\mathbf{c_1 c_2}^H = 0 \tag{2.1}$$

The reason that it is important to have orthogonal beams is as follows. When two beams are orthogonal, a feeding network can be used to connect these beams to different inputs, that are uncoupled from eachother. For the transmit array this means that when one input is excited, no signal will go to the other inputs. For the receive array this means that when a beam pattern is received that is matched to one of the outputs, all power will go to this output. Furthermore, the receive feeding structure can be designed such that internal reflections have no impact. So to formulate the requirement for the transmit and receive excitation coefficients, suppose that $\mathbf{t_{c1}}$, $\mathbf{t_{c2}}$ and $\mathbf{t_{c3}}$ are the excitation coefficients for the three transmit beams, and that $\mathbf{r_{c1}}$, $\mathbf{r_{c2}}$, $\mathbf{r_{c3}}$ and $\mathbf{r_{c4}}$ are the excitation coefficients for the four receive beams. The orthogonality requirements for the transmitter excitation coefficients and for the receiver excitation coefficients are as follows:

$$\mathbf{t_{ci} t_{cj}}^H = 0 \text{ for any } i, j \text{ with } i \neq j \tag{2.2}$$

$$\mathbf{r_{ci} r_{cj}}^H = 0 \text{ for any } i, j \text{ with } i \neq j \tag{2.3}$$

It can be checked that the coefficients given in table 2.1 and 2.2 do not fulfill these requirements. To fix this, lossy networks are added in the feeding networks. This is not good, but necessary to have good beam patterns. The additional power can be removed from the array by placing absorbers on the printed circuit board, or can be removed via the back plate of the antenna. More information on the lossy networks is given in chapters 4 and 5.

3

Transmission line technology and components

The goal of this chapter is to discuss the transmission line technology that is used and to show the different components used in the final design. The chapter is built up as follows. Section 3.1 discusses the properties of the used transmission line technology. Section 3.2 talks about the losses of the transmission line technology. Section 3.3 shows the different components used in the final design. Simulated properties of these components are also shown.

3.1. Properties substrate integrated waveguide

In this section the used transmission line technology and its properties will be given. The used transmission line technology is substrate integrated waveguide (SIW) [18–25]. A SIW line is made by placing rows of vias in a dielectric substrate. This is shown in figure 3.1. The rows of vias behave as a waveguide, even though the rows are not full metal walls. The dimensions of the waveguide are selected such that only the TE_{10} mode propagates. Above and below the substrate, metal layers are placed to make sure the propagating mode is contained.

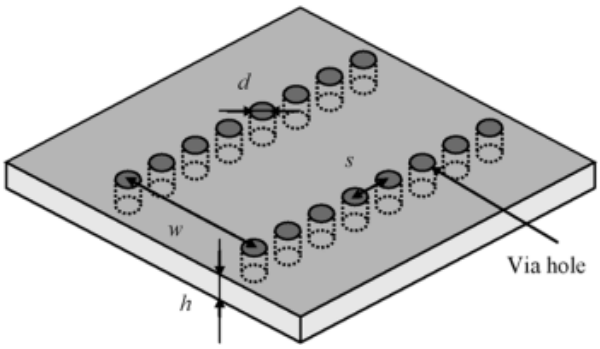

Figure 3.1: A schematic overview of SIW transmission line technology. Provided by dr. J. Puskely, also used in [19].

One parameter of a SIW line is the width w. The width should be larger than 0.5 times the wavelength in the dielectric, to make sure the TE_{10} mode can propagate. Other parameters are the thickness of the substrate h, the via spacing s, the via diameter d and the thickness of the metal layers t_{metal}. These parameters should be selected such that production constraints are met. Furthermore, s and d should be selected such that the propagating mode is contained within the waveguide, also see [20]. The ϵ_r of the substrate is selected such that the wavelength in the dielectric is not too much smaller than the wavelength in the dielectric. This makes sure that a subarray can be designed that has good bandwidth properties. Furthermore, the material that is selected also determines the loss properties.

Table 3.1 shows the parameter values that were selected. Additionally, the center frequency f_c, the wavelength in air λ and the wavelength in the substrate $\lambda_{dielectric}$ are also given.

Table 3.1: SIW properties for this project.

w	6.25 mm
h	0.787 mm
s	0.9 mm
d	0.5 mm
t_{metal}	35 μm
Material	Rogers RT5880
ϵ_r	2.2
f_c	24.1 GHz
λ_{air}	12.4 mm
$\lambda_{dielectric}$	8.4 mm

It should be noted that the final design will be a two-layer SIW structure. This means that SIW lines can be placed on the bottom layer and on the top layer. This gives more room to implement different feeding structures.

3.2. Losses in substrate integrated waveguide

At the design frequency of 24.1 GHz, losses in the SIW-lines can be important. Losses become even higher when the frequency increases. The goal of this section is to give an idea how big the impact of the losses is.

A calculation is done to determine how large the losses are. This calculation assumes that there is a regular waveguide filled with a dielectric, instead of a SIW line. This approximation is deemed good enough for now. The approach was learned in [26]. The losses in the waveguide can be divided in two parts. The first part is losses in the dielectric. The second part is losses due to currents in the walls of the waveguide. Figure 3.2 shows a plot of the losses in the waveguide for different waveguide widths a. One line shows the losses in the dielectric, another line shows the losses in the waveguide walls, and the last line shows the total losses.

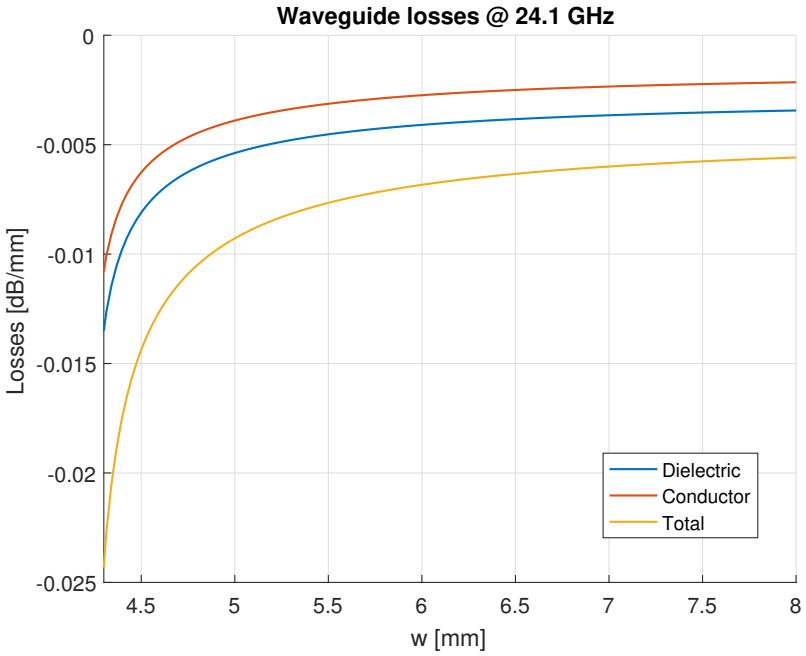

Figure 3.2: Loss properties of a waveguide filled with a dielectric, for different widths of the waveguide w.

A marker is placed at approximately the width that is used in the final design. At this point, the losses are 0.0066 dB/mm. This corresponds to 0.66 dB of losses for every 10 cm. This is not yet a very big problem, but this does show that losses are not necessarily negligible. The losses will be even more significant when the frequency is higher.

3.3. Components

The final antenna design is built up out of many different components. The goal of this section is to show the different components. The components that are discussed are the hybrid coupler, layer transition, Y power divider, T power divider, crossover and antenna subarray. The hybrid coupler is an important part of the Butler matrix. The layer transition is used to move a SIW line from the bottom layer to the top layer or vice versa. The power dividers are used to distribute the power among the radiating elements. The crossover is used to cross two SIW lines that are on the same layer, and can be used in the Butler matrix and in the rest of the distribution network. The antenna subarray is a row of slots that radiate power into free space. In chapter 4 and 5 will be shown in more detail how the components are used. In the rest of this section, the properties for each component are given, and the lay-out and CST model are shown. The S-parameters that are obtained via simulation of the CST-model are also shown.

3.3.1. Hybrid coupler

A main component of the design is the hybrid coupler. This component is also the main part of the Butler matrix. The hybrid coupler has two input ports and two output ports. Both the inputs are matched, and they are uncoupled from eachother. This component therefore provides the option to distribute power from one input to the antenna elements, without coupling to other inputs. Often a -3 dB hybrid is used. In this case equal power goes to both outputs. One output has a 90 degree phase shift with respect to the other output.
The implementation of the hybrid coupler was provided by dr. J. Puskely. Figure 3.3a shows the implementation of the -3 dB hybrid in a MATLAB plot. The two inputs are port 1 and 2, and the two outputs are port 3 and 4. The two sets of protruding via walls provide equal distribution of power to both outputs. Furthermore, when one input is active, all signal towards the other input is cancelled. There is no coupling between the inputs.
Figure 3.3b shows the CST implementation. It can be seen that the CST model mostly matches the MATLAB plot. One difference is that in the CST model, some metal struts are placed near the ports. This is only for simulation purposes. Figure 3.4 show the S-parameters that are obtained with the CST simulation. Only port 1 is activated, but this gives all information, since the structure is symmetrical. It can be seen that the reflection and the coupling with the other input are both below -30 dB. The power that goes to both outputs is approximately -3 dB.

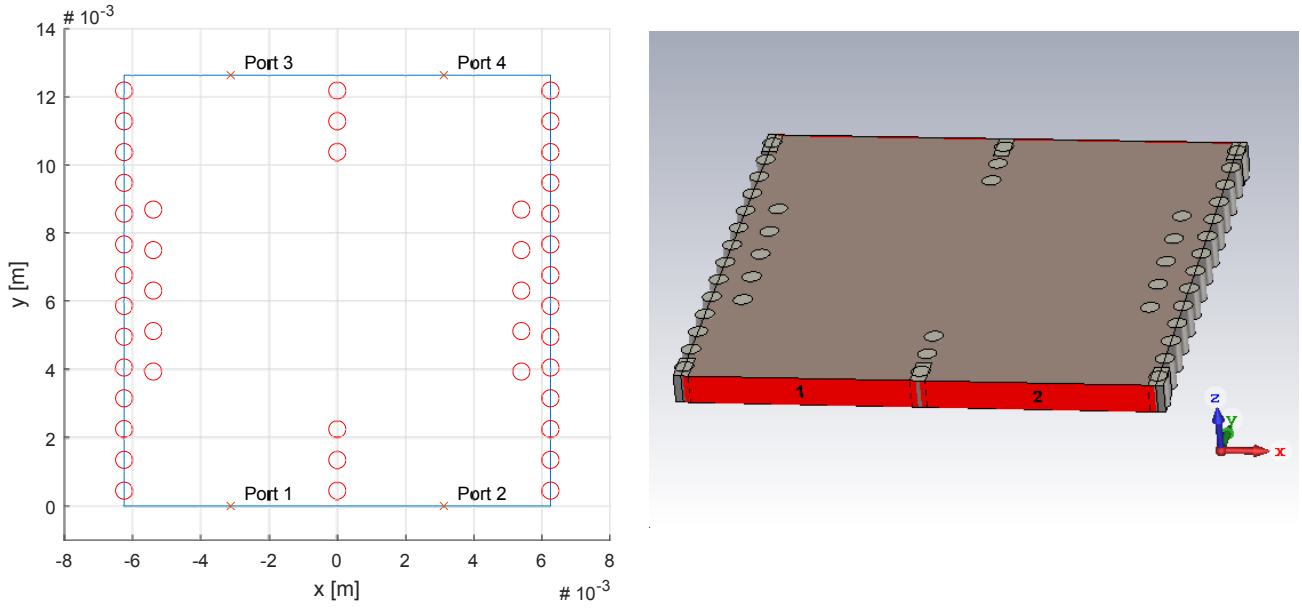

(a) MATLAB lay-out (b) CST model

Figure 3.3: Implementation of an equal power hybrid coupler.

Instead of having a -3 dB hybrid, it is also possible to create an asymmetrical hybrid. In this case, the power that goes to one output is larger than the power that goes to the other output. Such an asymmetrical hybrid

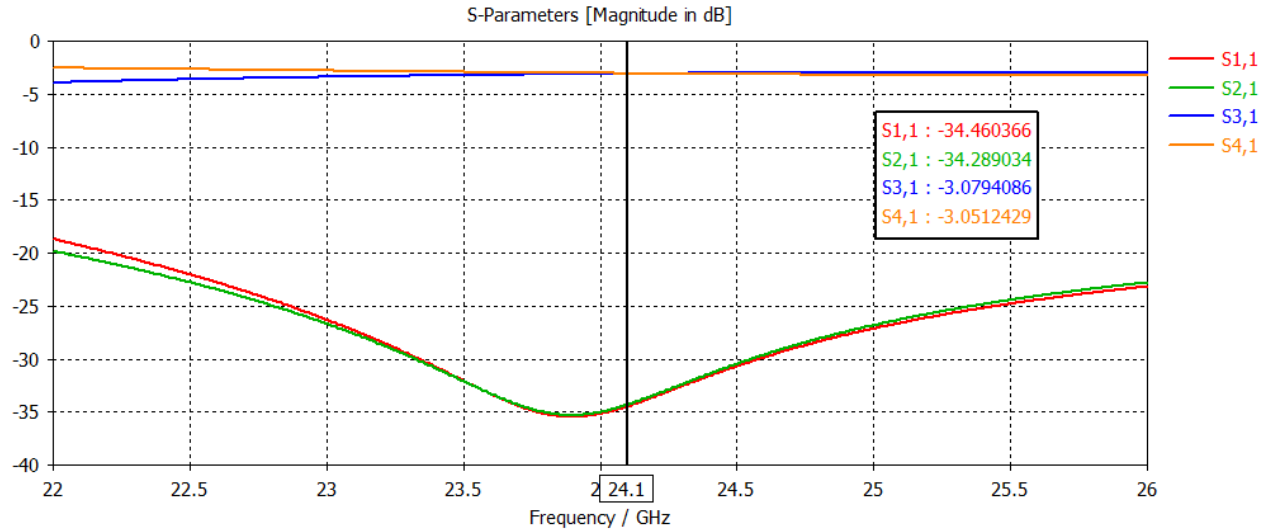

Figure 3.4: The simulated S-parameters of the equal power hybrid coupler.

can be created by adjusting the via spacing and the location of the protruding via walls. These asymmetrical hybrids can be used to remove some part of the power from a line. They have as advantage that the line is then still matched from both sides. In the final design, some power attenuation is required. To remove the power in this case, asymmetrical hybrids are used.

3.3.2. Layer transition

The final design consists of two SIW layers. To move a SIW line from the bottom to the top or vice versa, a layer transistion is required. Figure 3.5a shows the implementation in a MATLAB plot, and Figure 3.5b shows the CST-model. It can be seen that a transversal slot is used to transfer the power between the layers. Figure 3.6 shows the simulated S-parameters. It can be seen that the reflection is less than -30 dB.

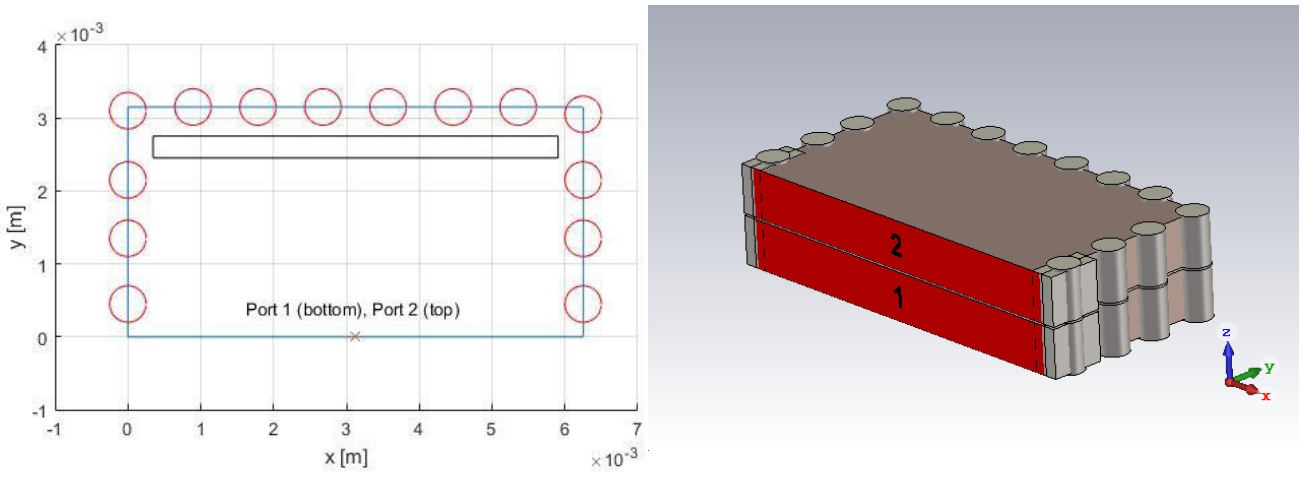

(a) MATLAB lay-out (b) CST model

Figure 3.5: Implementation of the layer transition.

3.3.3. Y power divider

It can be desirable to divide the power in one SIW line, over two SIW lines. This can be done using a power divider. Depending on the position of a power divider in the final design, it may be desirable to have a certain shape of power divider [27, 28]. Two shapes are investigated. In this subsection the Y power divider is investigated, and in the next subsection the T power divider is investigated.

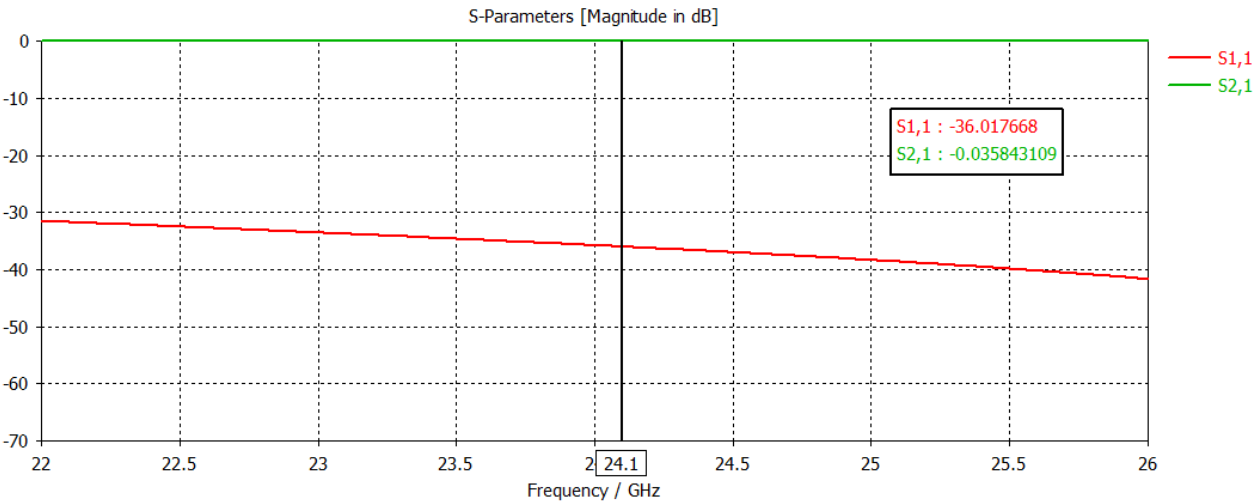

Figure 3.6: The simulated S-parameters of the layer transition.

Figure 3.7a shows the implementation of the Y power divider in a MATLAB plot. Figure 3.7b shows the CST model. This specific case is for equal power division. The input line is split into two output lines. The two seperated vias in the bottom left corner and bottom right corner are used for matching. Figure 3.8 shows the simulated S-parameters. The matching is below -30 dB.
Different power divisions can be made by changing the position of the row of vias between the two output lines.

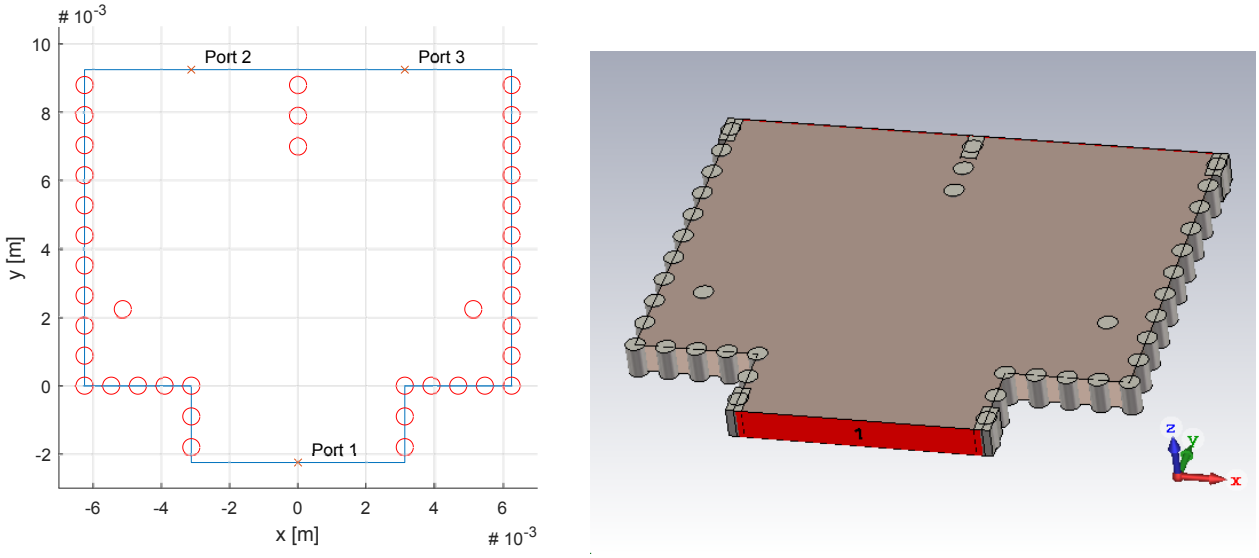

(a) MATLAB lay-out

(b) CST model

Figure 3.7: Implementation of the Y power divider.

3.3.4. T power divider

It is also possible to create a power divider in a T shape. Figure 3.9a shows the implementation of the T power divider in a MATLAB plot. Figure 3.9b shows the CST model. This specific case is for equal power division. The bottom port is the input, and the left and right ports are the outputs. The seperated via is placed for matching. Figure 3.12 shows the simulated S-parameters. The matching is below -30 dB. Different power divisions can be made by changing the position of the seperated via.

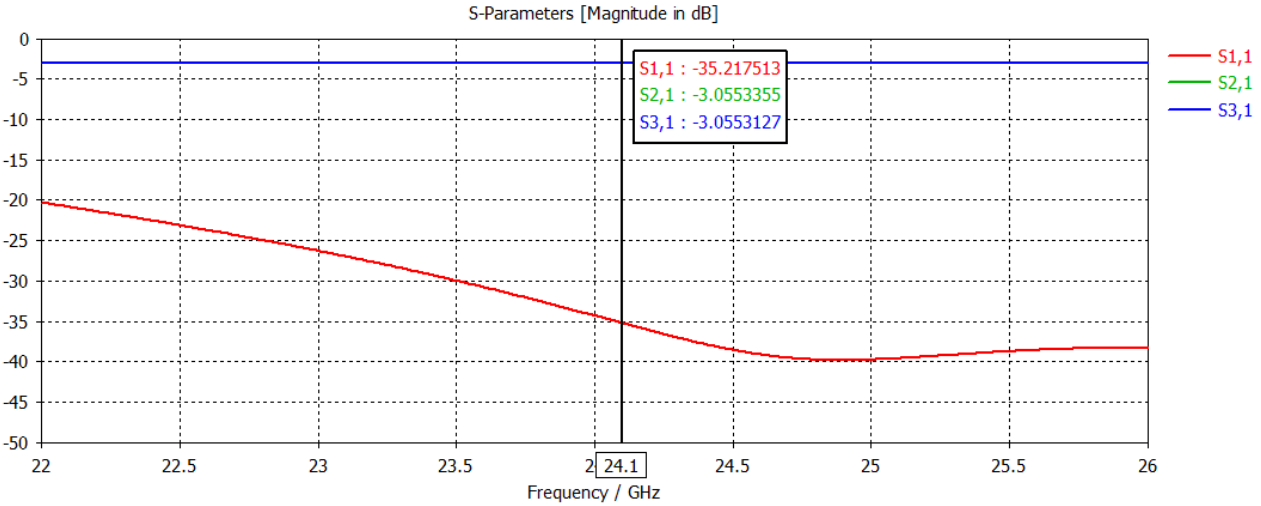

Figure 3.8: The simulated S-parameters of the Y power divider.

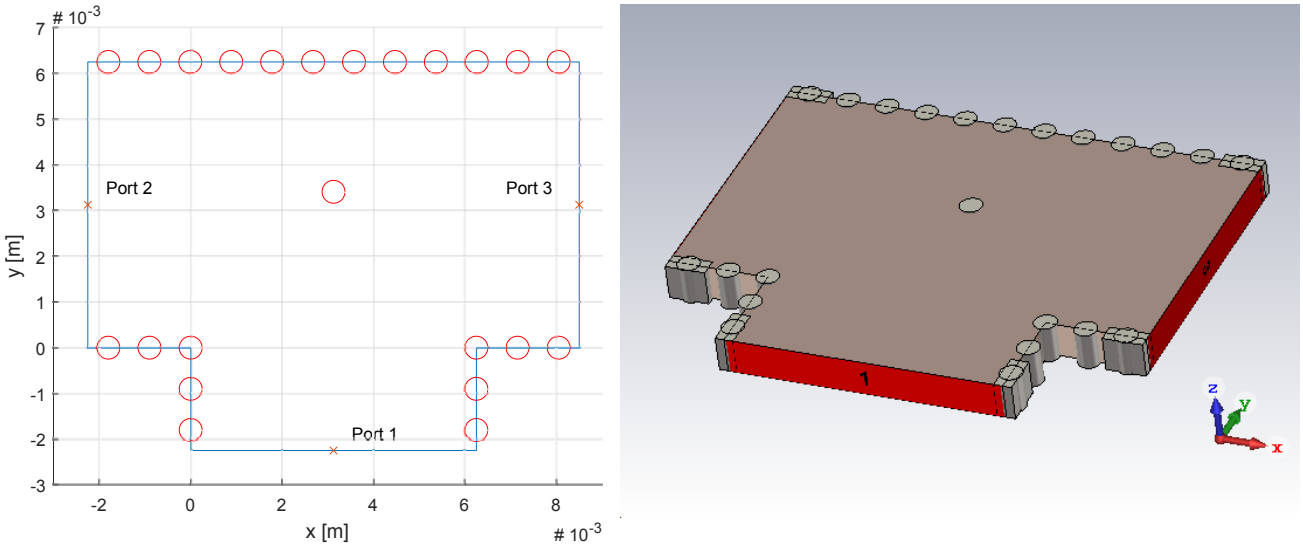

(a) MATLAB lay-out (b) CST model

Figure 3.9: Implementation of the T power divider.

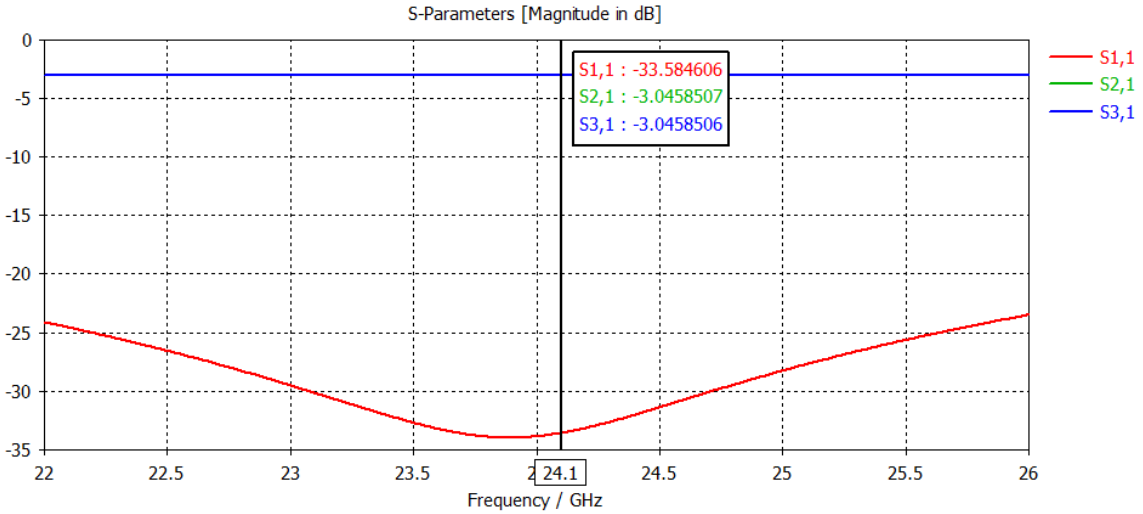

Figure 3.10: The simulated S-parameters of the T power divider.

3.3.5. Crossover

It may be required to cross two SIW lines that are on the same layer. This can be done using the crossover component. A crossover can be made by concatenating two of the -3 dB hybrids in subsection 3.3.1. The phase distribution of the -3 dB hybrids then ensures that all signal crosses to the other side. Signals that stay on the same side are cancelled. The implementation of the crossover was provided by dr. J. Puskely. Figure 3.11a shows the implementation of the crossover in a MATLAB plot. Figure 3.11b shows the CST model. Figure 3.12 shows the simulated S-parameters. It can be seen that all power goes from the activated input port, to the output port diagonally across from this port. All other S-parameters are below -30 dB.

3.3.6. Subarray

The antenna subarray is the component that contains the radiating elements. The radiating elements are longitudinal slots in the top of the SIW lines. Power inside a SIW line can leak to the outside through these slots. To create good matching of the antenna subarray, it is possible to change the displacement of the slots from the center of the SIW line. More information on waveguide slot antennas is given in [29–32].
Every subarray consists of 10 radiating elements. This is required to obtain an elevation beam pattern that is directive enough. All slots have the same displacement from the center of the SIW line. Therefore, the subarrays have uniform amplitude tapering. This means that a single subarray has a sidelobe level in the elevation direction of approximately -13 dB. When the transmit and receive array are combined, this results in a SLL of approximately -26 dB, which is sufficient.
The antenna subarray is one of the most critical components in terms of matching and bandwidth. It is difficult to obtain matching that is below -20 dB. The bandwidth is limited, because the propagating wave inside the SIW line needs to resonate with both the radiating slot at the beginning of the line and the radiating slot at the end of the line. This means that the wavelength may not vary too much.
An implementation of the subarray was provided by dr. J. Puskely. Figure 3.13a shows the implementation of the subarray in a MATLAB plot. Figure 3.13b shows the CST model. Figure 3.14 shows the simulated S-parameters. It can be seen that the matching is not even -20 dB. The -10 dB bandwidth is 0.75 GHz. This can be made larger, by decreasing the amount of radiating slots. This would then come at the cost of reduced directivity in the elevation beam pattern.

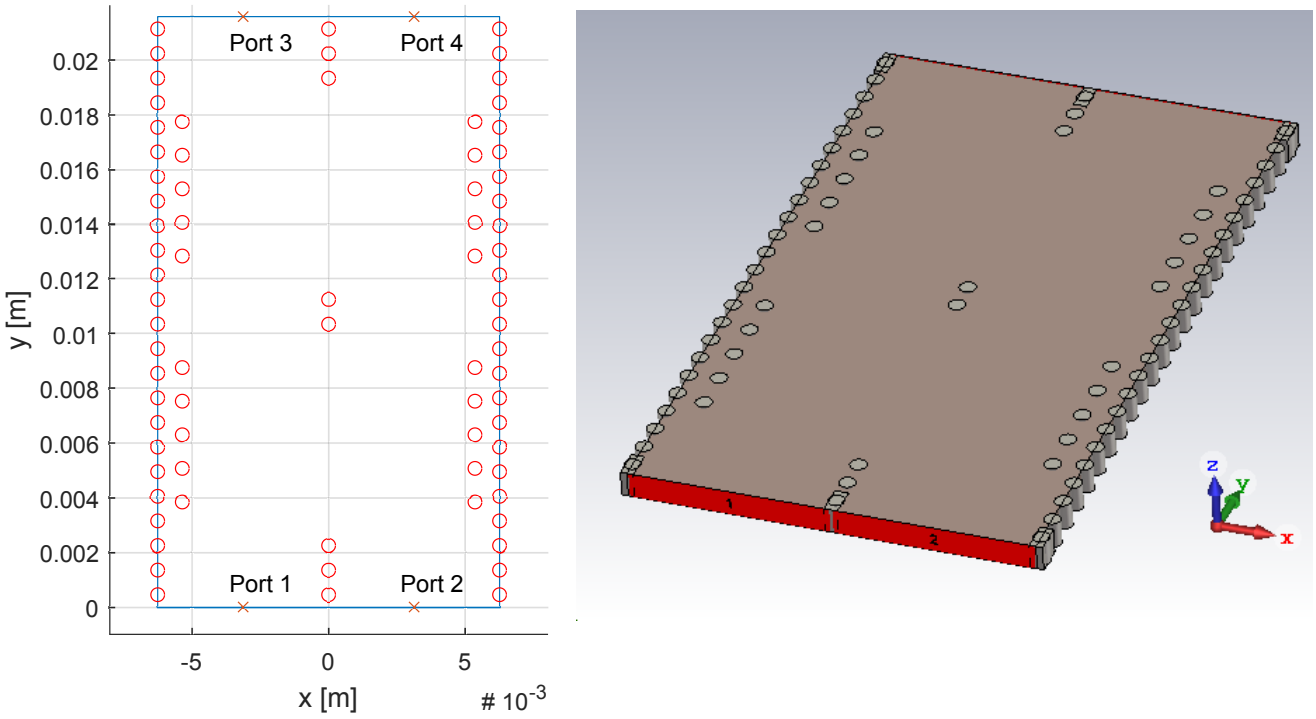

(a) MATLAB lay-out

(b) CST model

Figure 3.11: Implementation of the crossover.

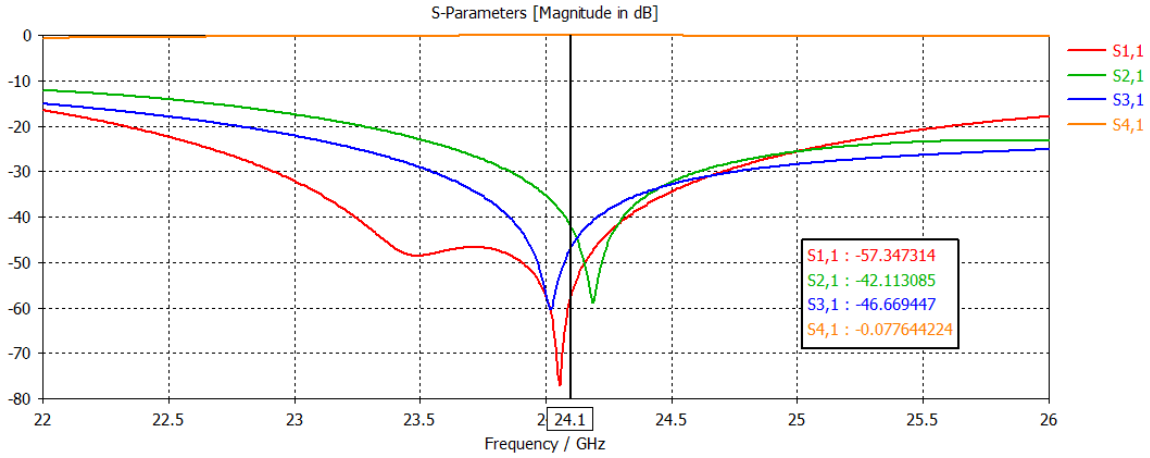

Figure 3.12: The simulated S-parameters of the crossover.

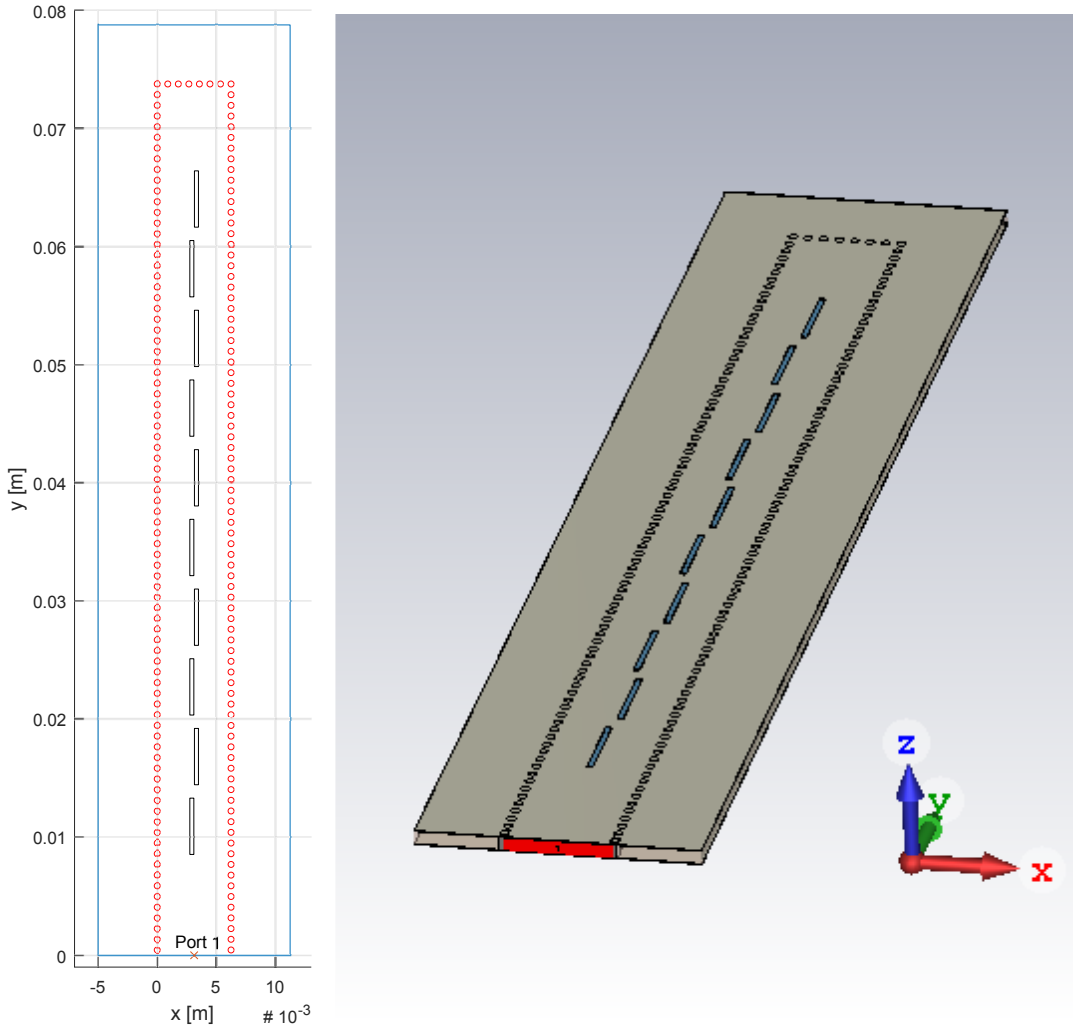

(a) MATLAB lay-out

(b) CST model

Figure 3.13: Implementation of the subarray.

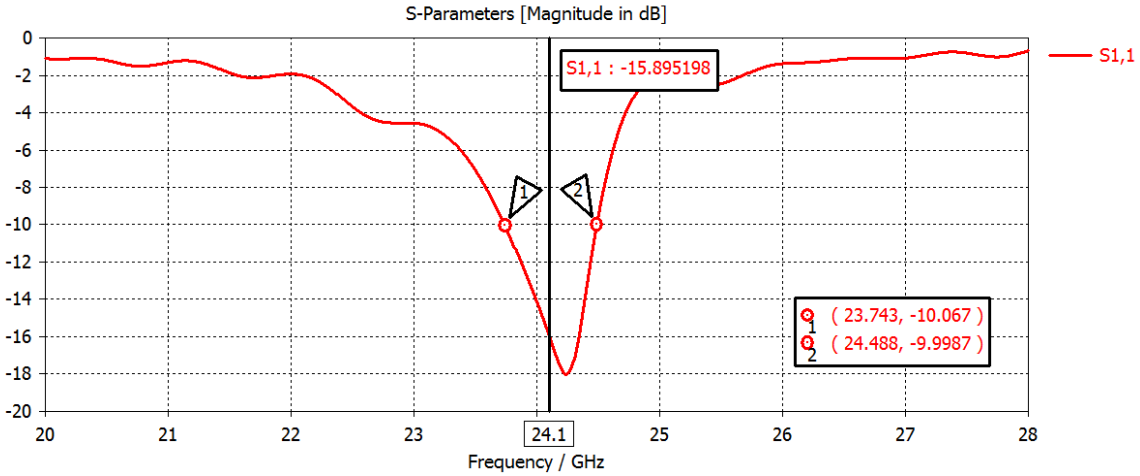

Figure 3.14: The simulated matching of the subarray.

Figure 3.15 shows the simulated beam pattern in the elevation direction at the center frequency. The beam stays the same up to a reasonable amount over the bandwidth where there is matching. The SLL is -11.8 dB. The -3 dB beamwidth is 10.7 degrees. When the transmit and receive array will be combined, the total SLL and -3 dB beamwidth will be better than these values.

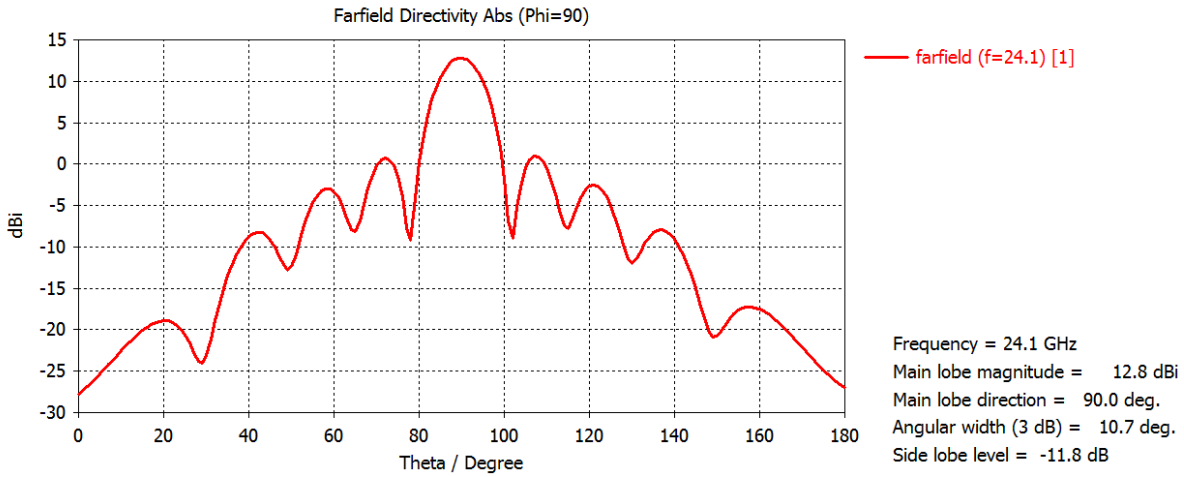

Figure 3.15: The farfield elevation beam pattern of the subarray at the center frequency.

Figure 3.16 shows the simulated beam pattern of the subarray in the azimuth direction at the center frequency. The full array will probably have a larger metal plane around the radiating elements than the CST-model for the subarray. Nevertheless, the beam pattern simulation can give an indication how the subarray will behave. It can be seen that the directivity is relatively constant over a large part of the total field of view, as might be expected for radiating slots. At the edges of the field of view, the directivity becomes a bit lower.

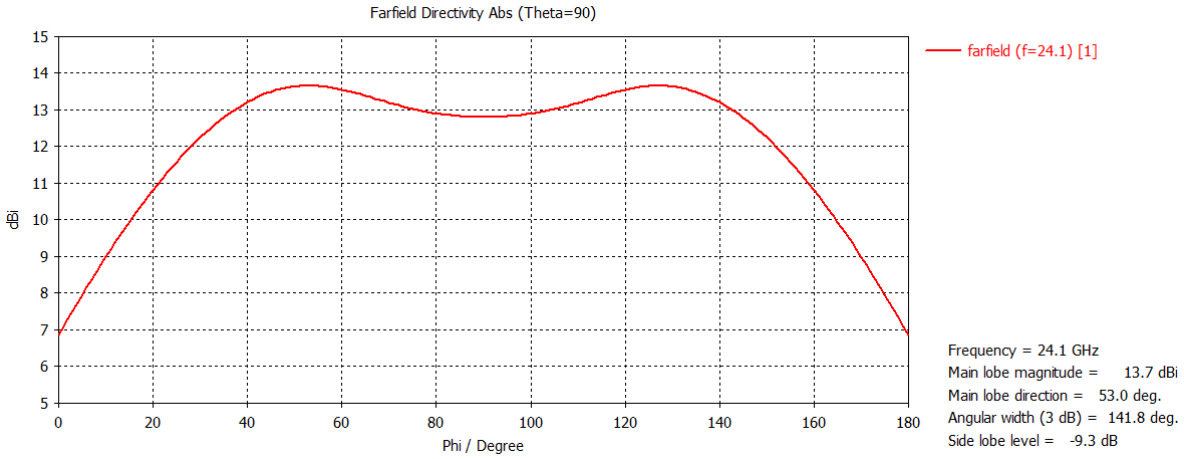

Figure 3.16: The farfield azimuth beam pattern of the subarray at the center frequency.

4

Transmit array

In this chapter the full design of the transmit array, including the beamforming network, are shown. The transmit array should realise the beam patterns given in chapter 2, section 2.3. The array is also simulated, and the results are analysed.
The chapter is built up as follows. In section 4.1 is explained why power attenuators are used. In section 4.2 the implementation of the transmit array in MATLAB is shown. Finally, in section 4.3, the CST model of the transmit array is shown. This CST model is simulated, and the simulation results are discussed.

4.1. Beam orthogonality

The goal of this section is to explain why power attenuators are used in the transmit beamforming network. Table 4.1 repeats the table that was given in chapter 2, section 2.3. This table contains the coefficients with which the antenna elements are activated. The transmit beamforming network should create these excitation coefficients. As mentioned before in chapter 2, section 2.5, it is important that the possible vectors with excitation coefficients are orthogonal to eachother. This does not hold for the coefficients in table 4.1.

To solve this problem, power attenuators are placed between the transmit beamforming network, and the antenna elements. This makes it possible to adjust the excitation coefficients in such a way, that they are orthogonal. In the final design, a power attenuator of -4.3 dB is placed before antenna elements 1 and 6. This means that the beamforming network has to create the excitation coefficients that are given in table 4.2, which are orthogonal to eachother. The adjusted coefficients are marked in red. So the coefficients in table 4.1 are the coefficients after the power attenuators, and the coefficients in table 4.2 are the ones before the power attenuators.

4.2. Implementation MATLAB

The goal of this section is to show the design of the transmit beamforming network, and to explain how the network works. First, a schematic overview of the design is given. After this, the lay-out with the correct placement of the components is shown. Finally, the design with placement of the vias is shown.
Figure 4.1 shows a schematic overview of the transmit beamforming network. For explanation, this network is divided in two parts, as indicated.

Part 1. The first part is a 4-input Butler matrix, of which only 3 of the input ports are used. Usually the progressive phase shifts at the end of the Butler matrix are $-90°$, $-45°$, $45°$ and $90°$. An additional $45°$ progressive phase shift is added at the end of the Butler matrix, using phase shifters. This means that

Table 4.1: Progressive phase shifts and amplitude coefficients for the different transmit channels.

	β	$\lvert t1\rvert$	$\lvert t2\rvert$	$\lvert t3\rvert$	$\lvert t4\rvert$	$\lvert t5\rvert$	$\lvert t6\rvert$
Channel 1	$-90°$	0.595	1.018	1.387	1.387	1.018	0.595
Channel 2	0	0.595	1.018	1.387	1.387	1.018	0.595
Channel 3	$90°$	0.595	1.018	1.387	1.387	1.018	0.595

Table 4.2: Progressive phase shifts and amplitude coefficients for the different transmit channels, before the power attenuators.

	β	$\|t1\|$	$\|t2\|$	$\|t3\|$	$\|t4\|$	$\|t5\|$	$\|t6\|$
Channel 1	$-90°$	0.981	1.018	1.387	1.387	1.018	0.981
Channel 2	0	0.981	1.018	1.387	1.387	1.018	0.981
Channel 3	$90°$	0.981	1.018	1.387	1.387	1.018	0.981

for the three inputs, the progressive phase shifts are $-90°$, $0°$ and $90°$, as is desired. At the end of part 1, the SIW lines have uniform amplitude coefficients.

Part 2. The second part consists of the distribution of the signal over the antenna elements. One output of the Butler matrix is connected to elements 1 and 5, using a power divider. The same thing is done in [9, 33, 34]. This gives the possibility to connect a larger aperture, and to have some amplitude tapering. The same thing is done for antenna elements 2 and 6. Antenna elements 3 and 4 are each connected to one output of the Butler matrix in part 1. Finally, in the SIW lines that connect to antenna elements 1 and 6, the power attenuators are added, as was explained in section 4.1.

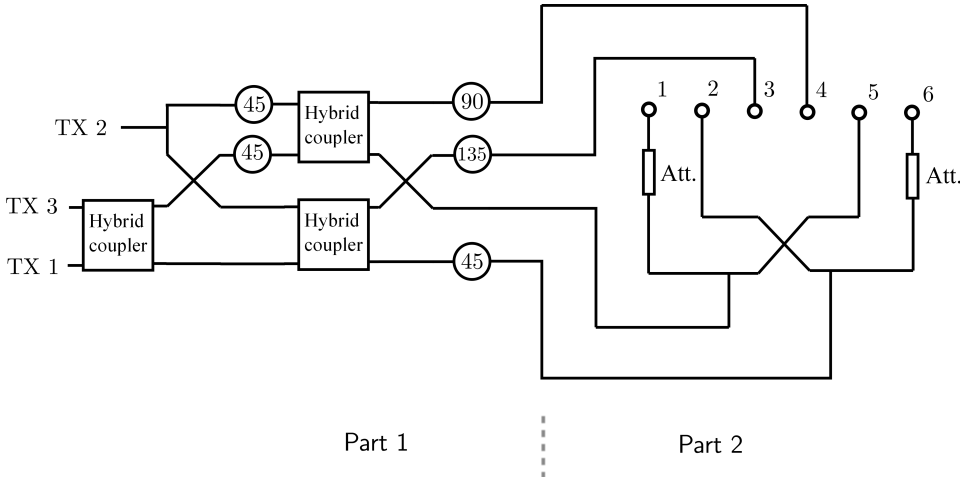

Figure 4.1: A schematic that shows the lay-out of the transmit beamforming network.

Figures 4.2 and 4.3 show a more detailed implementation of the schematic in figure 4.1. The components discussed in chapter 3 are placed here in the correct locations. The drawn sizes of the components match the actual sizes. All components in the figures are given labels, and the labels are explained in the legends.
Figure 4.2 shows the detailed lay-out of the bottom layer of the transmit array. The input ports are shown on the left, and are marked TX1, TX2 and TX3. After this, all components up to and including the two adjacent hybrid couplers are part of the Butler matrix. The rest of the components give the distribution of the SIW lines among the antenna elements. For all power dividers and asymmetrical hybrids, the division ratio is given. At the top and bottom of the figure are the layer transitions that are used to move to the top layer.

Figure 4.3 shows the detailed lay-out of the top layer of the transmit array. This layer only contains the antenna subarrays.

Next, for the lay-outs given in figures 4.2 and 4.3, the component blocks are replaced by the vias. Figure 4.4 shows the implementation of the bottom layer with vias. It can be seen that there is a direct match with the lay-out in figure 4.2. Again, the input ports are marked. Additionally, the ports are marked where a matched load should be placed. At these ports, an asymmetrical hybrid was used to remove power from the SIW line. The removed power should go to a matched load. The matched loads themselves were not implemented in the design. Different options to create a matched load may be as follows. It may be possibly to replace some part of the dielectric with a more lossy material. It may also be possible to remove power by creating some holes in the back of the PCB. Figure 4.5 shows the implementation of the top layer with vias. Again, there is a direct match with the lay-out in figure 4.3. The locations of the radiating slots are also plotted. It can be seen that the slots in the even subarrays are mirrored, compared with the slots in the odd subarrays. This is to compensate that even subarrays are fed from negative y-values and that odd subarrays are fed from positive y-values.

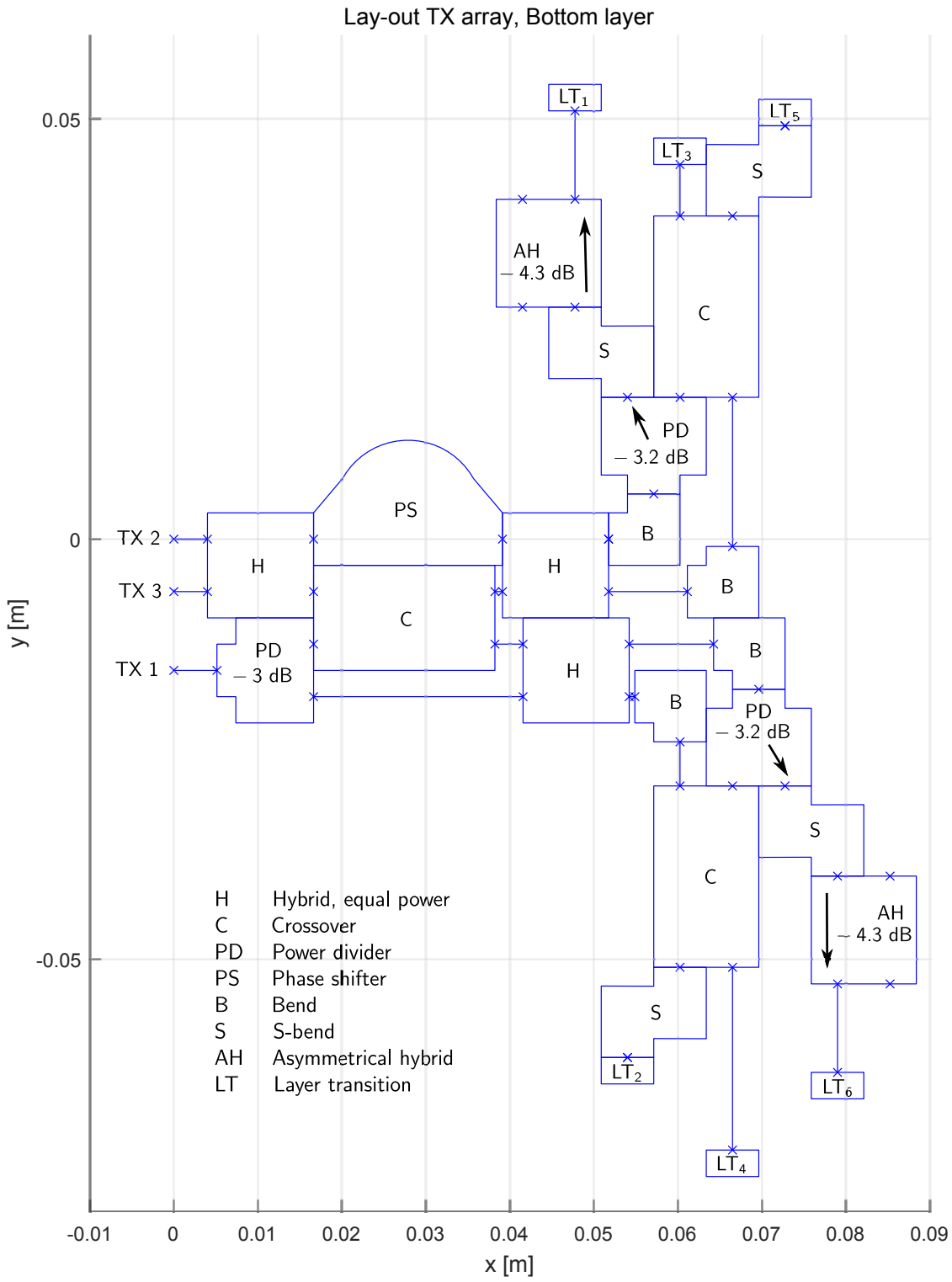

Figure 4.2: The precise component layout of the bottom layer of the transmit array.

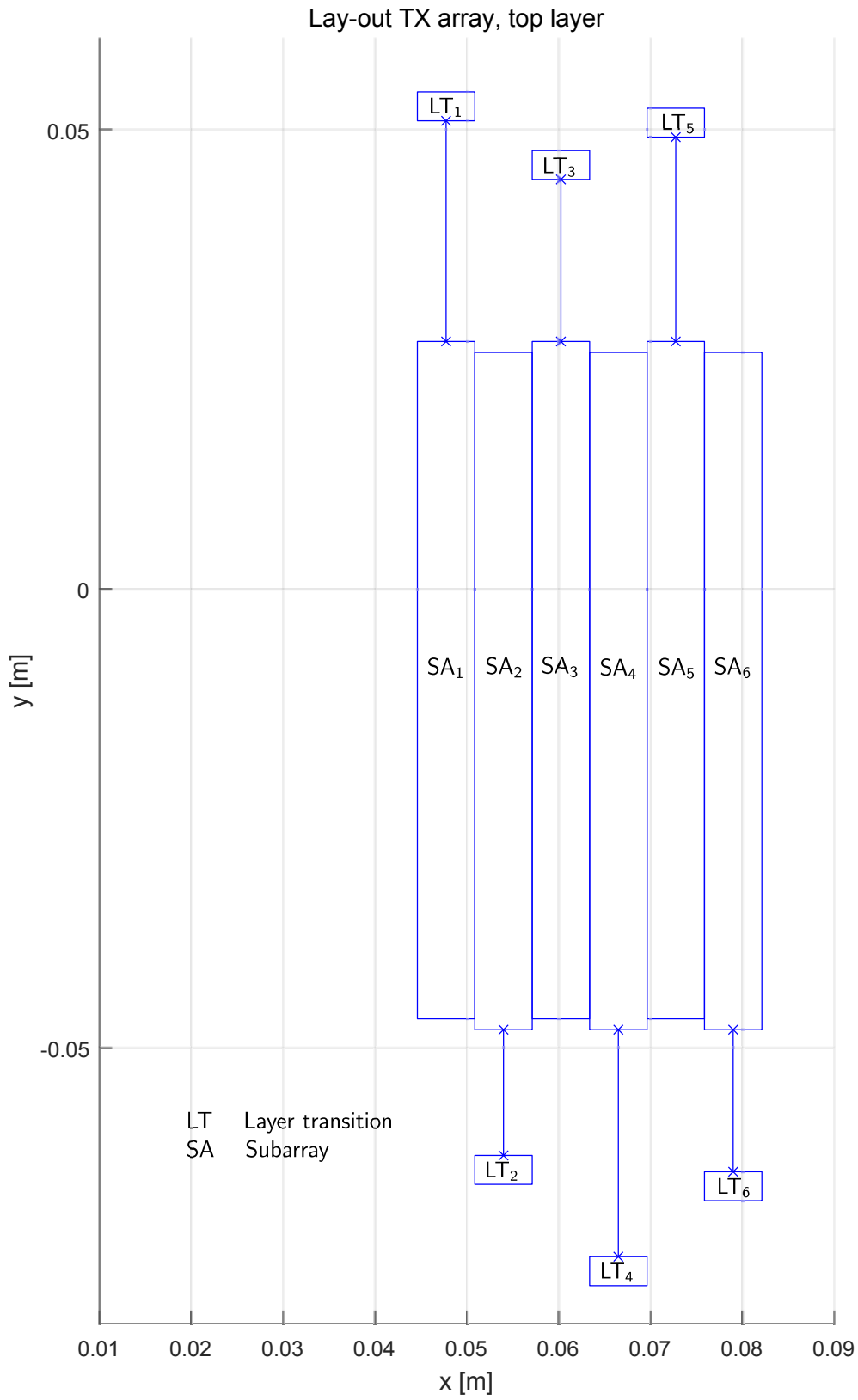

Figure 4.3: The precise component layout of the top layer of the transmit array.

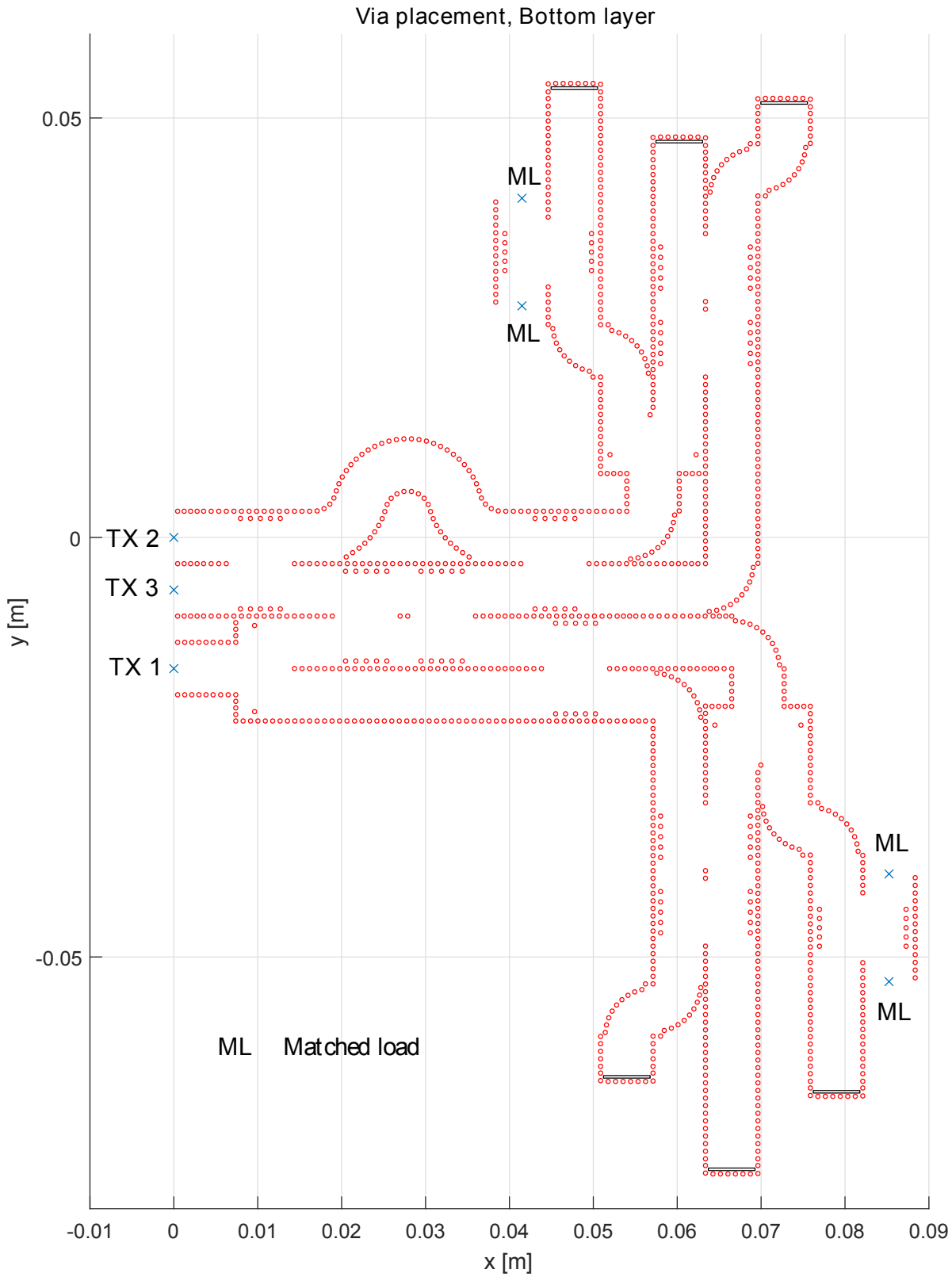

Figure 4.4: The implementation of the bottom layer of the transmit array with vias.

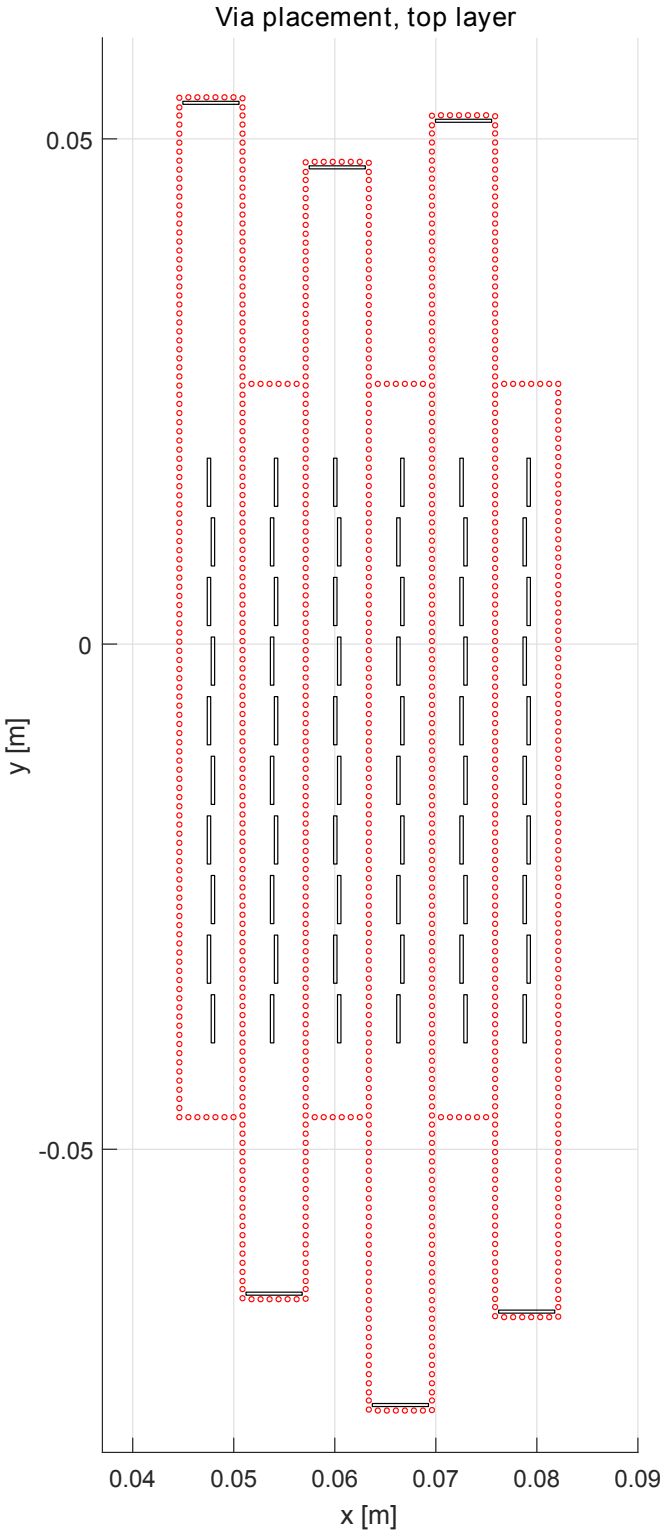

Figure 4.5: The implementation of the top layer of the transmit array with vias.

4.3. CST simulation

The goal of this section is to show the CST model of the transmit array, and to show the simulation results that were obtained with this model.
Figure 4.6 shows the CST model of the bottom layer. There is a direct match with figure 4.4. In this model, the dielectric is only placed where necessary, to save simulation time. If the design was to be produced, a larger slab of dielectric would be used. Figure 4.7 shows the CST model of the top layer. There is a direct match with figure 4.5. Figure 4.8 shows the full CST model, with the bottom layer and the top layer combined.

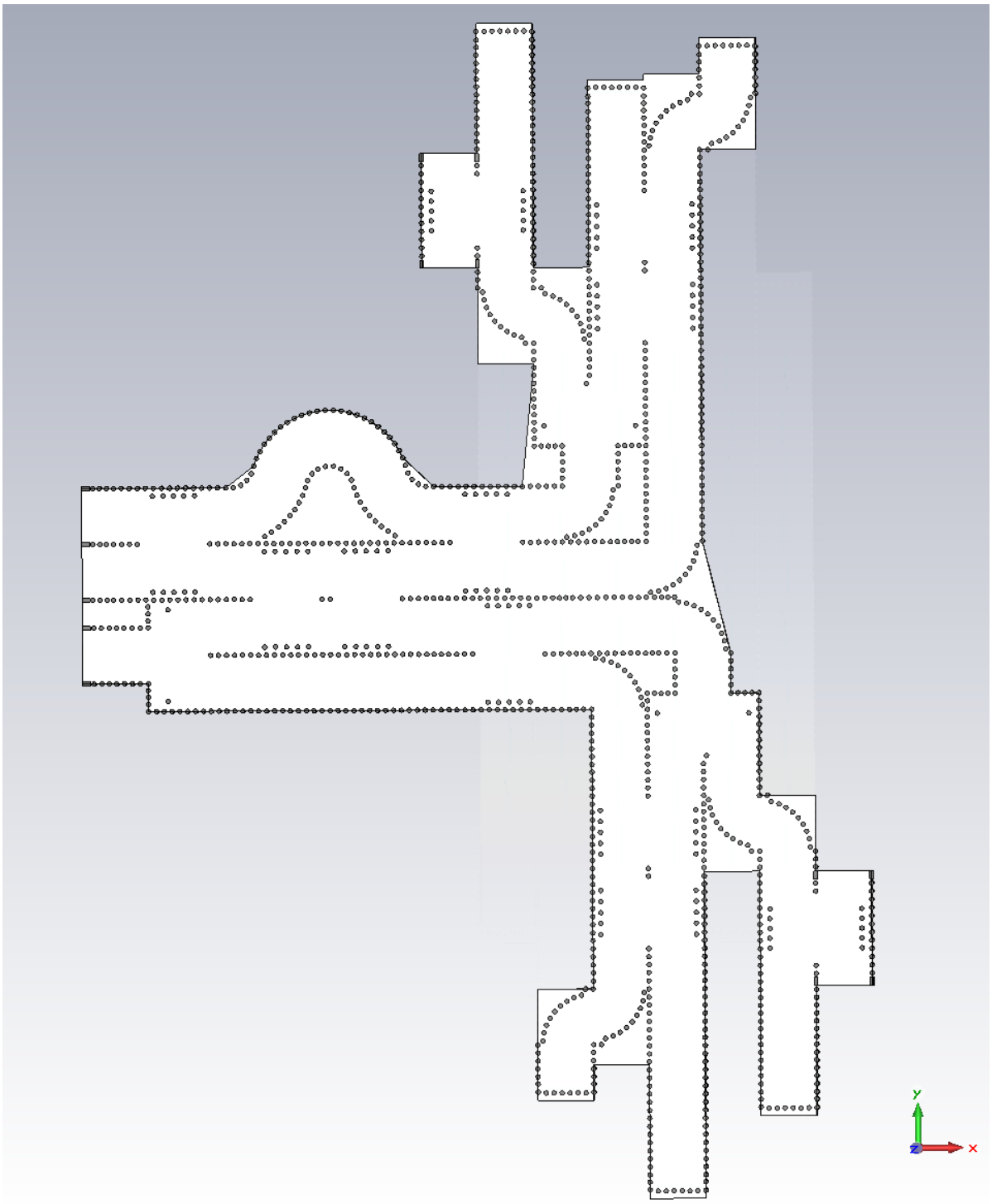

Figure 4.6: The CST model of the bottom layer of the transmit array.

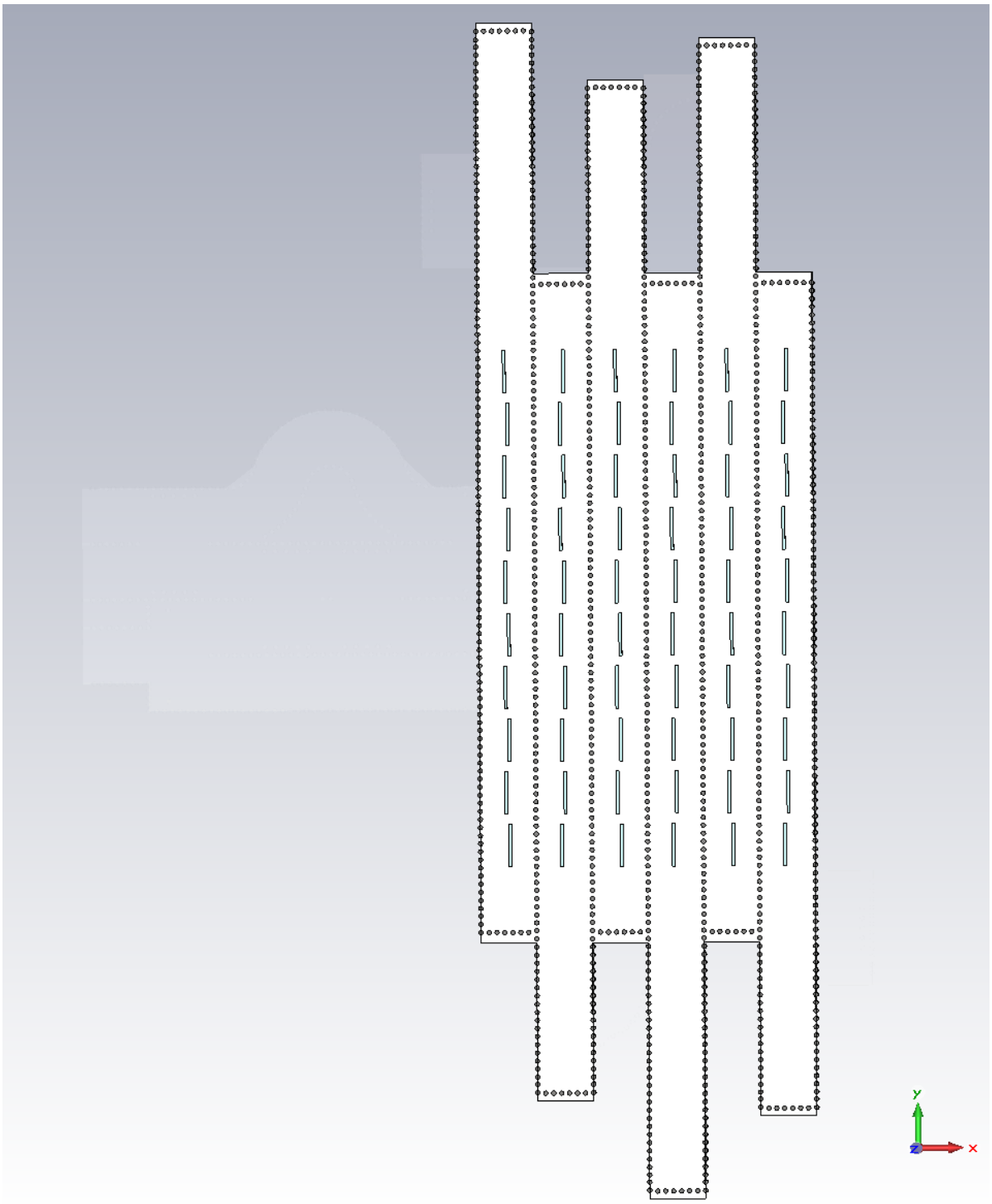

Figure 4.7: The CST model of the top layer of the transmit array.

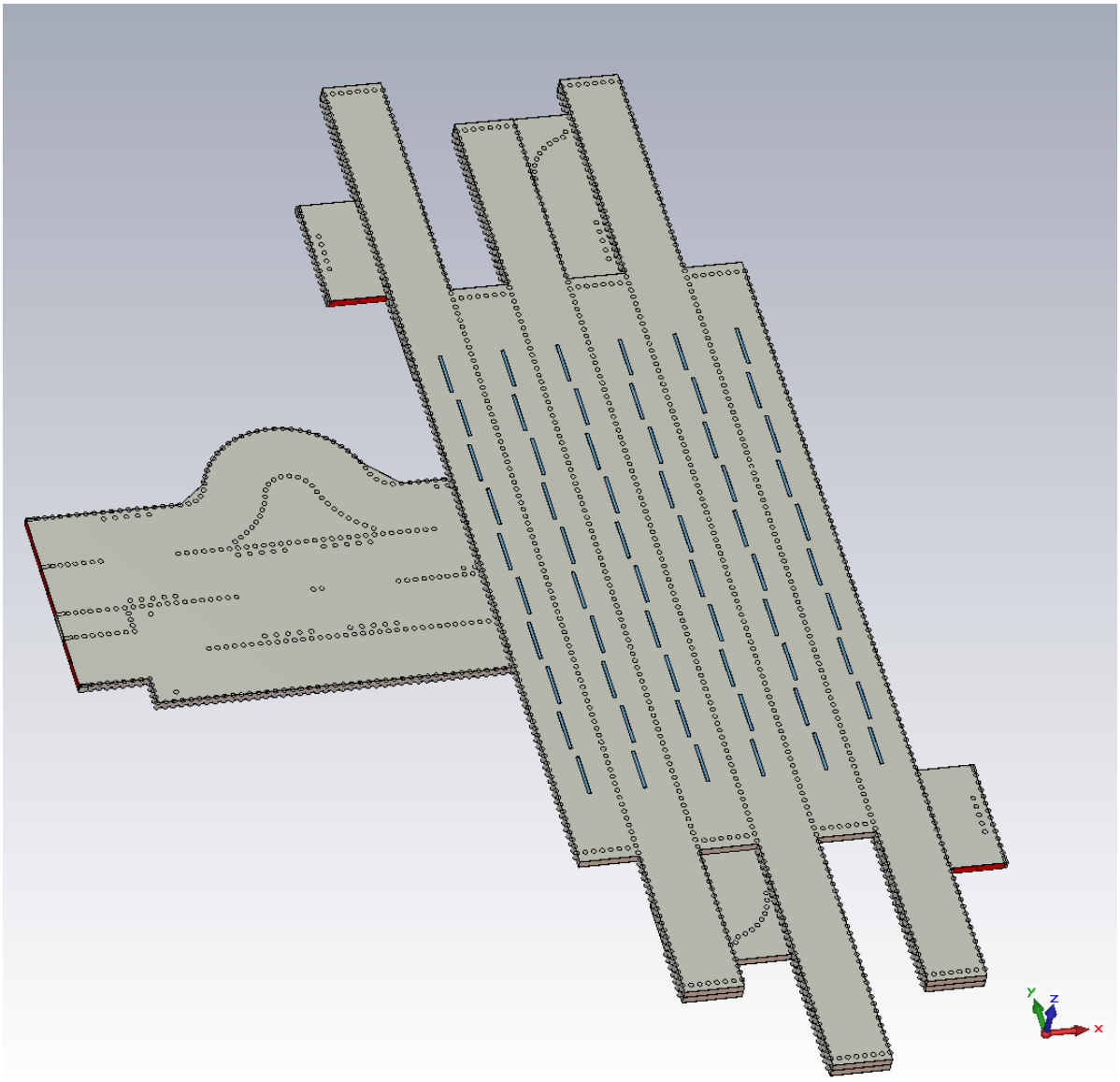

Figure 4.8: The full CST model of the transmit array.

The full CST model was simulated. Figure 4.9 shows the beam patterns that were obtained using the simulations. The desired beam patterns are also shown. These were originally given in 2, section 2.3. It can be seen that there is a good match between the desired beams and the simulated beams. The simulations have some sidelobes that are slightly too high. This is the worst for channel TX1. The results are accepted for now.

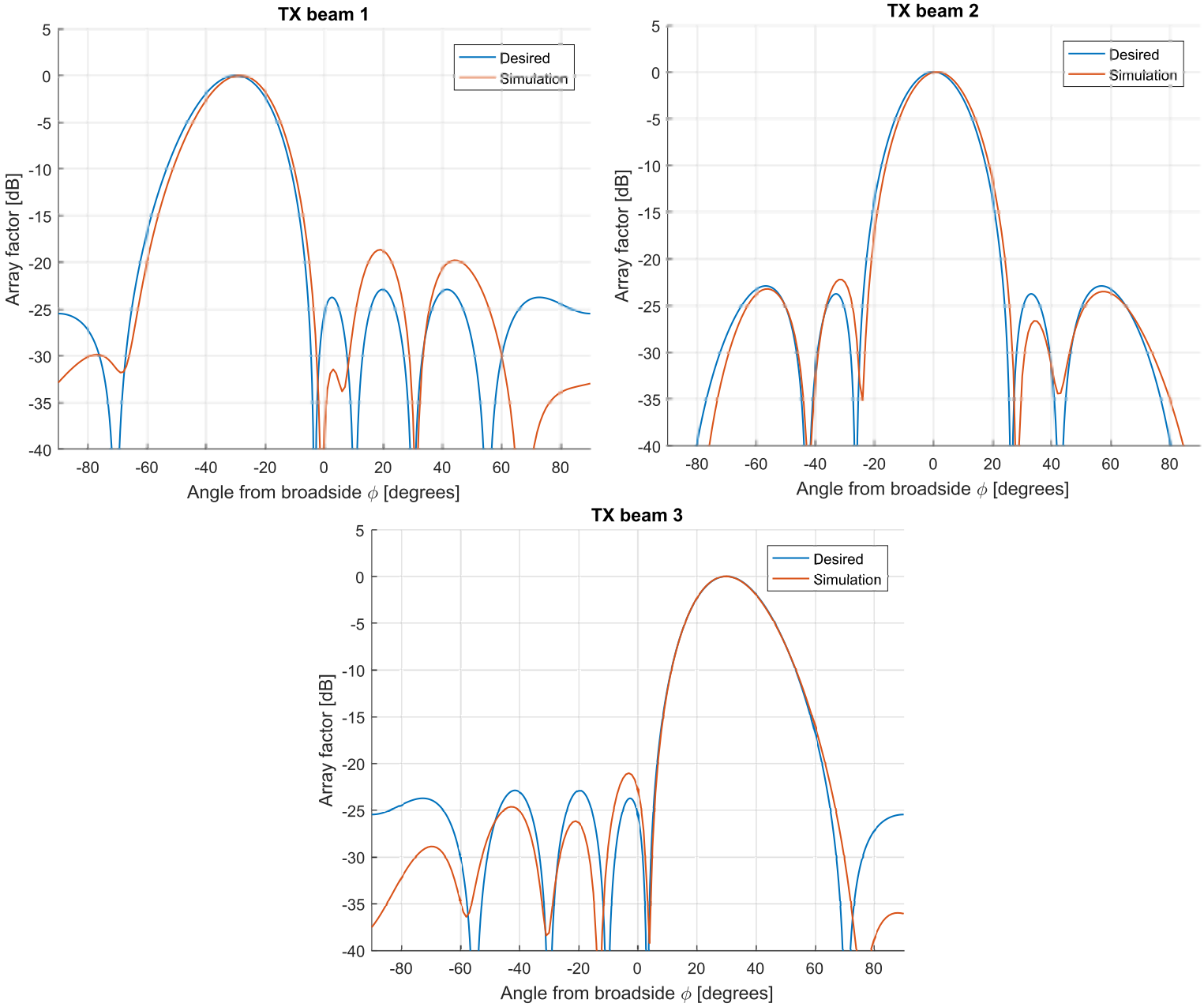

Figure 4.9: The transmit beam patterns, that are simulated using the CST model.

To give an idea of the matching, some of the reflection coefficients of the input ports are shown in figure 4.10. The top left figure shows the reflection coefficient for input port TX1. In this case, the matching does not get below -15 dB. Furthermore, the bandwidth over which is at least below or near -10 dB is not very large. This reflection coefficient does not furfill the requirements. Nevertheless, due to time constraints, no further changes are made. The top right figure shows the reflection coefficient for input TX2. In this case the matching is below -15 dB, over a band of approximately 2.2 GHz. This means that the bandwidth ratio in this case is 9.3%. This matches the requirements given in chapter 1, section 1.3. The bottom part of the figure

shows the reflection coefficient for input TX3. This input is matched better than input TX2.

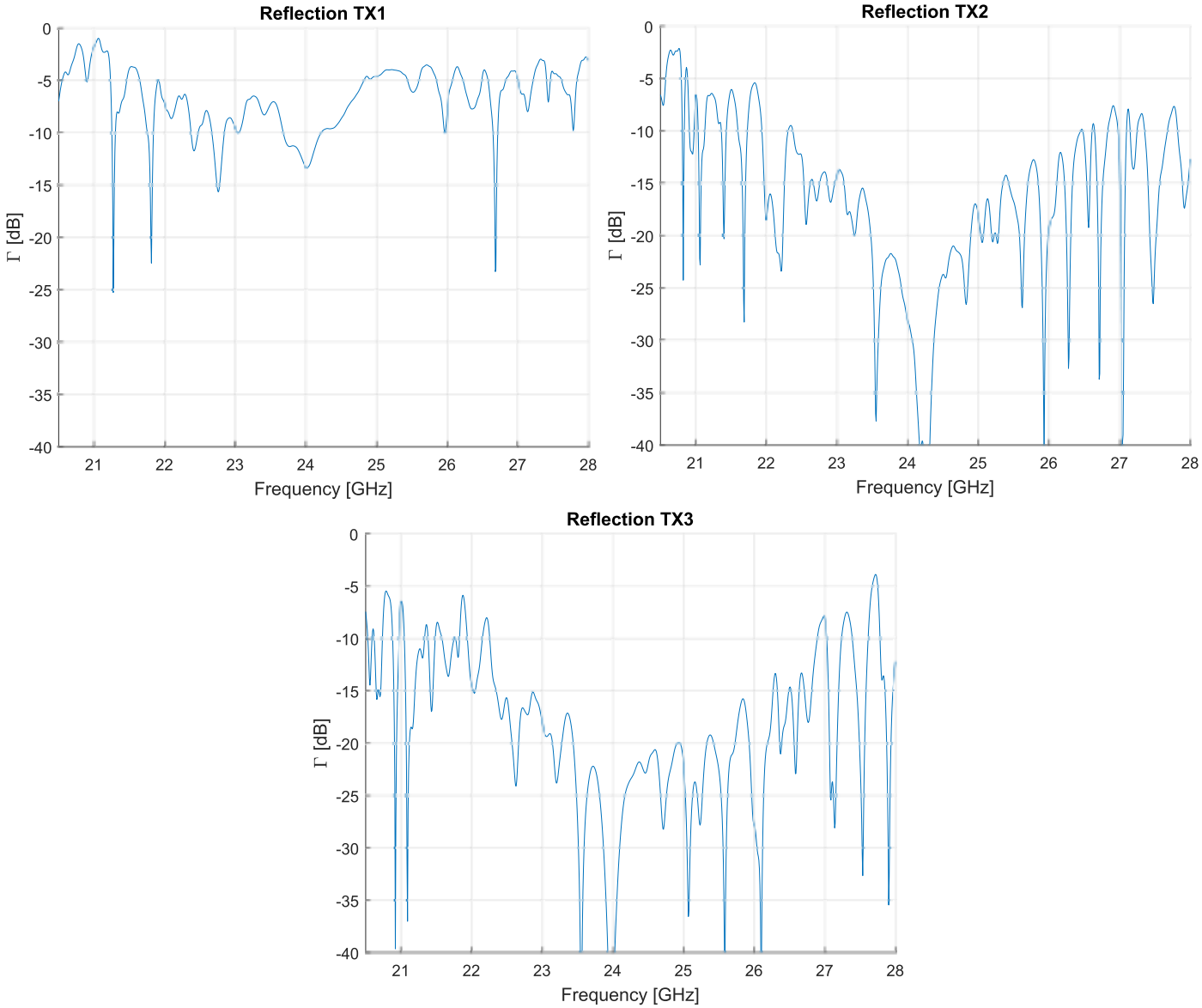

Figure 4.10: The reflection coefficients for the inputs to the transmit array.

5

Receive array

This chapter is built up in the same way as chapter 4, for the transmit array. In section 5.1 is explained why power attenuators are used. In section 5.2 the implementation of the receive array in MATLAB is shown. Finally, in section 5.3, the CST model of the receive array is shown. This CST model is simulated, and the simulation results are discussed.

5.1. Beam orthogonality

Just as for the transmit array, the receive beamforming network uses power attenuators. The power attenuators help to make sure that the beam coefficients that are created by the beamforming network are orthogonal. They are placed between the antenna elements and the beamforming network. Table 5.1 repeats the beam coefficients that are required to create the desired beam patterns. These were originally given in 2, section 2.3. Table 5.2 shows the beam coefficients after the power attenuation. The red numbers are the coefficients that are adjusted.
There is a difference between the transmit array and the receive array. For the transmit array, the power attenuators are placed in the SIW lines that go to the subarrays on the edges. For the receive array, the power attenuators are placed in the SIW lines that go to the center subarrays. The reason for this is that for the receive array the power is coming from the subarrays, instead of going towards the subarrays. When tapered beam coefficients are received, the center coefficients need to be attenuated to reduce the tapering. When the tapering is reduced, it is easier to create orthogonal coefficients.
The attenuation coefficients are as follows. SIW lines 3 and 7 are attenuated by 2.0 dB, SIW lines 4 and 6 are attenuated by 2.6 dB, and SIW line 5 is attenuated by 0.9 dB.

5.2. Implementation MATLAB

The goal of this section is to give a schematic overview of the receive array. Furthermore, more accurate MATLAB figures are shown, that show the exact location of different components. Finally, also the implementation with vias is shown.
Figure 5.1 shows a schematic overview of the receive array. For the explanation, the beamforming network is divided in two parts, as indicated in the figure.

Part 1. This part relates to the beamforming for channel 1 and 2. These channels connect to antenna subarrays 1, 3, 5, 7 and 9. The two channels are connected to a 4-port Butler matrix, of which only two of the ports

Table 5.1: Progressive phase shifts and amplitude coefficients for the different receive channels.

	β	$\|r1\|$	$\|r2\|$	$\|r3\|$	$\|r4\|$	$\|r5\|$	$\|r6\|$	$\|r7\|$	$\|r8\|$	$\|r9\|$
Channel 1	$-45°$	0.736	0	1.105	0	1.318	0	1.105	0	0.736
Channel 2	$45°$	0.736	0	1.105	0	1.318	0	1.105	0	0.736
Channel 3	$-90°$	0	0.627	0.911	1.266	1.393	1.266	0.911	0.627	0
Channel 4	$90°$	0	0.627	0.911	1.266	1.393	1.266	0.911	0.627	0

Table 5.2: Progressive phase shifts and amplitude coefficients for the different receive channels, after the power attenuators.

	β	$\|r1\|$	$\|r2\|$	$\|r3\|$	$\|r4\|$	$\|r5\|$	$\|r6\|$	$\|r7\|$	$\|r8\|$	$\|r9\|$
Channel 1	$-45°$	0.736	0	0.9920	0	1.0414	0	0.9920	0	0.736
Channel 2	$45°$	0.736	0	0.9920	0	1.0414	0	0.9920	0	0.736
Channel 3	$-90°$	0	0.627	0.8175	0.9393	1.1013	0.9393	0.8175	0.627	0
Channel 4	$90°$	0	0.627	0.8175	0.9393	1.1013	0.9393	0.8175	0.627	0

are used. After the two hybrid couplers, there are four SIW lines. These lines are distributed over the antenna elements using the rest of the feeding network. Subarray 1 and 9 are connected to the same output of the Butler matrix, similar to what was done for the transmit array. As mentioned in section 5.1, before the subarrays, some power attenuators are placed.

Part 2. This part relates to the beamforming for channel 3 and 4. These channels connect to antenna subarrays 2, 3, 4, 5, 6, 7 and 8. The two channels are connected to a single hybrid coupler. The two outputs of this hybrid coupler are distributed among the antenna elements using the rest of the feeding network. In the drawing, some dashed lines are used. These do not have a special meaning, but are only used to indicate that these SIW lines do not integrate with the solid SIW lines that are crossed. Again, some power attenuators are used.

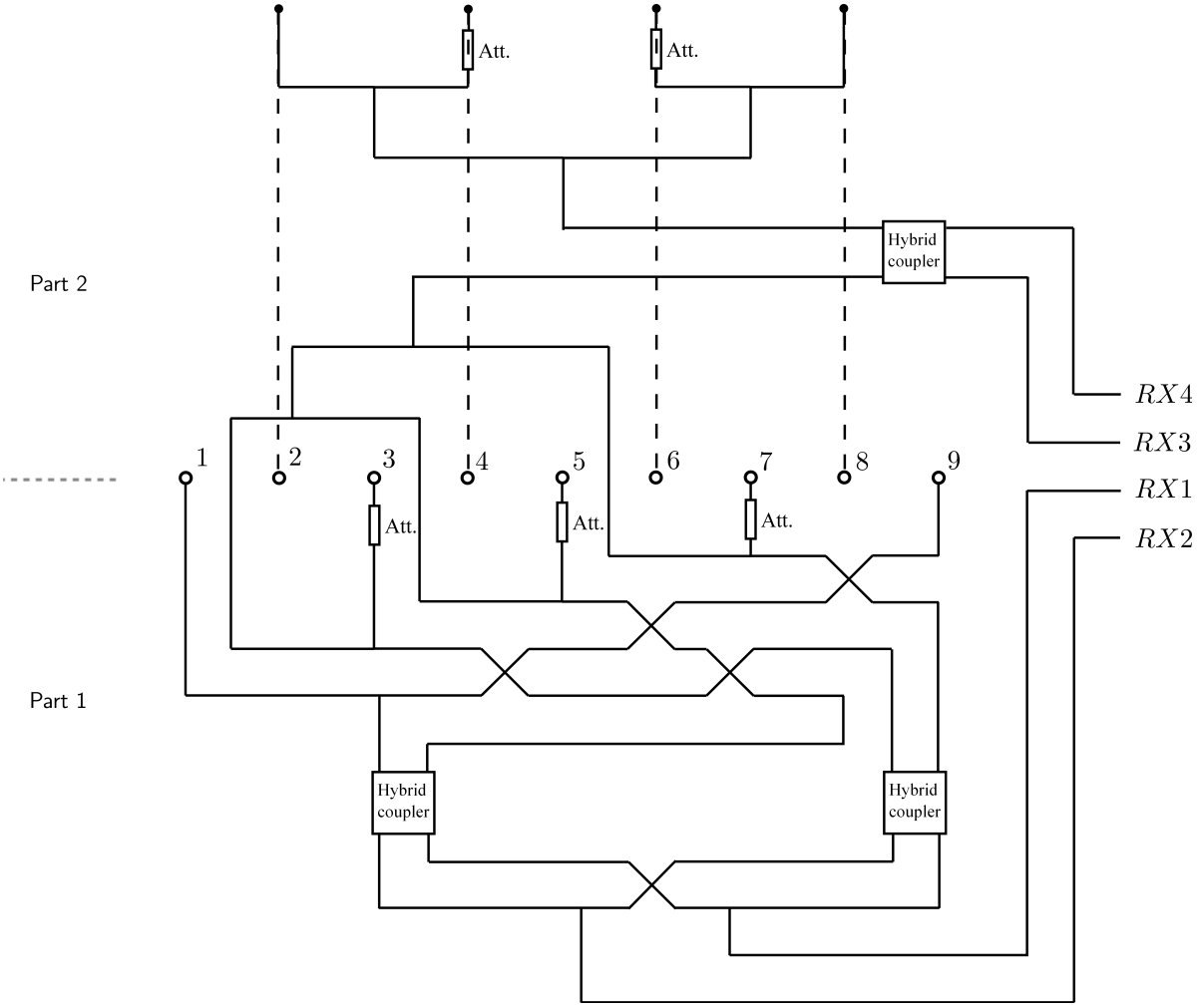

Figure 5.1: A schematic overview of the receive beamforming network.

Figures 5.2 and 5.3 show the effect on the feeding network when different channels are in use. The beam patterns that correspond to the different channels are also shown. The part of the feeding network that is

active, is shown in blue. Figure 5.2 shows the active part of the beamforming network for channel 1 and 2. It can be seen that since these channels connect to subarrays with 2λ spacing, the grating lobes are relatively close together. Figure 5.3 shows the active part of the beamforming network for channel 3 and 4. It can be seen that since these channels connect to subarrays with 1λ spacing, the grating lobes are relatively far apart.

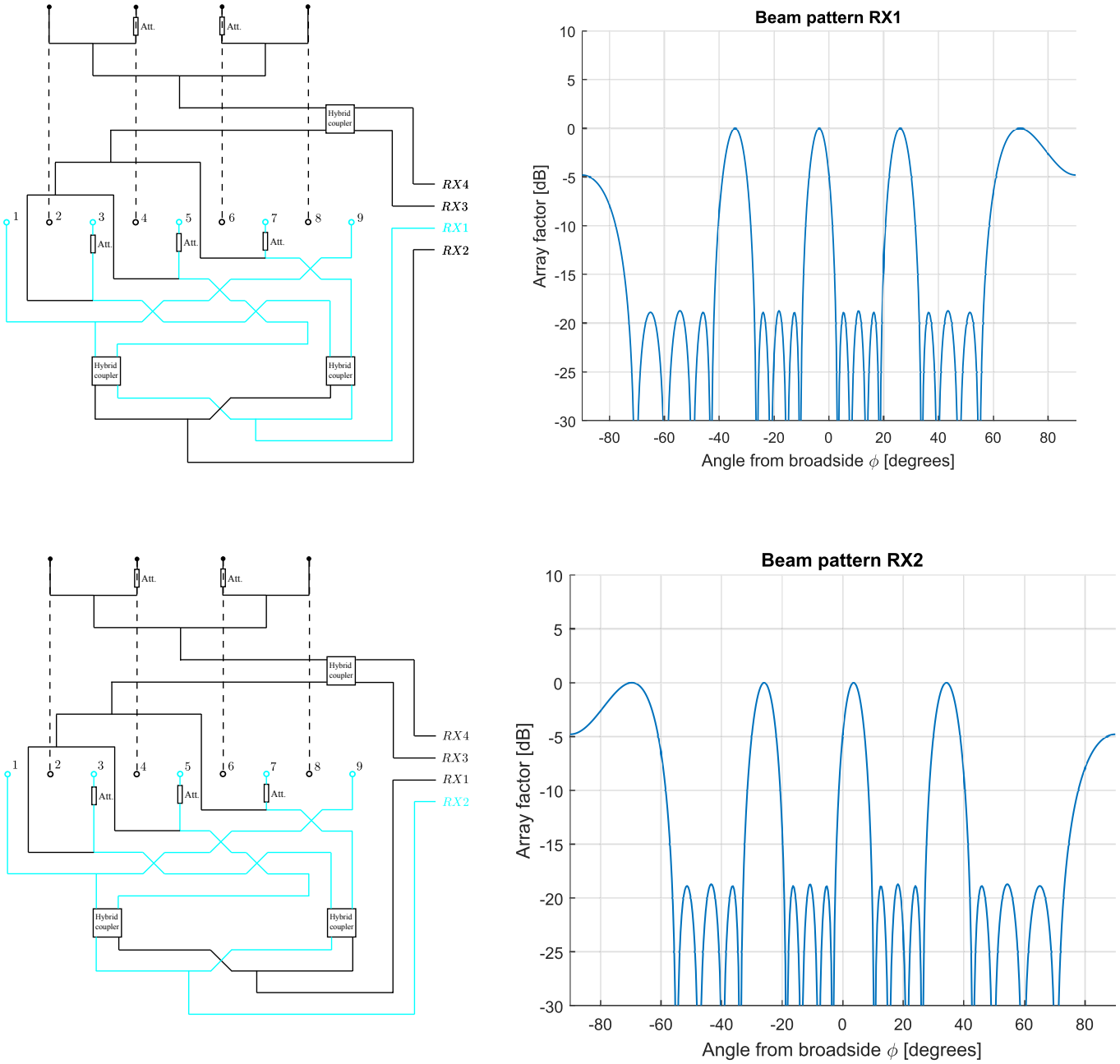

Figure 5.2: The parts of the beamforming network that are active, when different channels are in use. The corresponding beam patterns are also shown. The top figures are for channel 1, the bottom figures for channel 2.

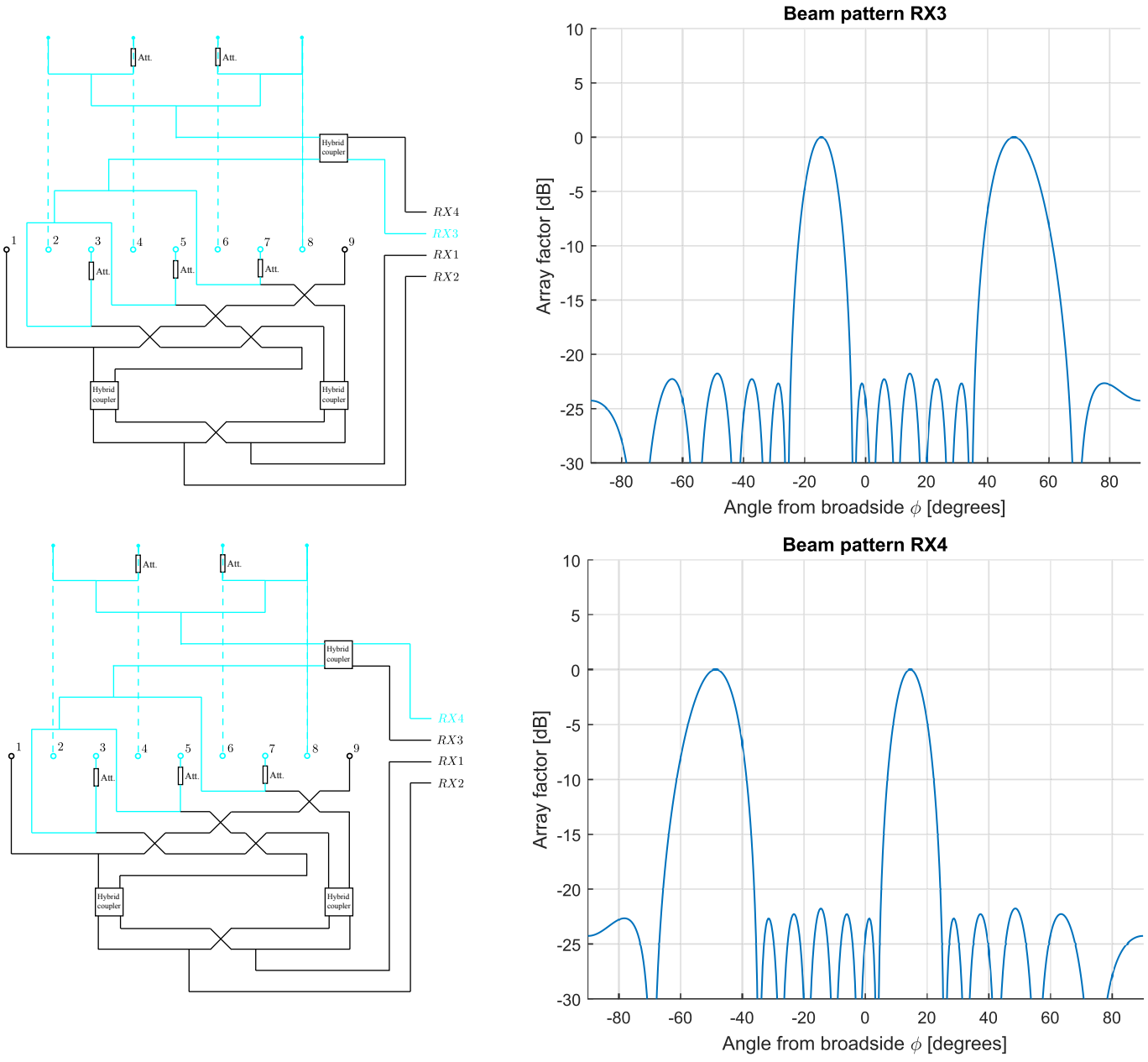

Figure 5.3: The parts of the beamforming network that are active, when different channels are in use. The corresponding beam patterns are also shown. The top figures are for channel 3, the bottom figures for channel 4.

Next, figures 5.4 and 5.5 show more detailed MATLAB figures, with precise locations of the different components. Labels are given to the different components. The division ratios of the power dividers and asymmetrical hybrids are also indicated. Furthermore, labels are placed next to the ports where the channels of the digital chip should be connected.
Figure 5.4 shows the component lay-out of the bottom layer of the final design. The bottom layer matches with part 2 in figure 5.1. It can be seen that after the connection for channel 3 and 4, there is the hybrid coupler. The rest of the network consists of distribution among the antenna elements.
Figure 5.5 shows the component lay-out of the top layer of the final design. The top layer matches with part 1 in figure 5.1. The connections for the two channels are shown at the bottom of the figure. After this, all components up to and including the two hybrid couplers, consists of the Butler matrix. The components after this provide the distribution of the antenna elements.
One special component shown in this figure is the custom power divider. This component combines part 1 and 2 in figure 5.1. The goal of this component is not to actually divide the power. If the beam pattern that is received by the array matches with one of the channels, all received power should go to that channel. All signal that goes to other branches of the beamforming network should be blocked. The custom power divider is tuned in such a way, that this is made possible.

Finally, figures 5.6 and 5.7 show the implementation of the receive array with vias. Figure 5.6 shows the implementation of the bottom layer with vias. It can be seen that there is a direct match with figure 5.4. Figure 5.7 shows the implmentation of the top layer with vias. It can be seen that there is a direct match with figure 5.5. In both figures, markers are placed at the locations where matched loads should be added.

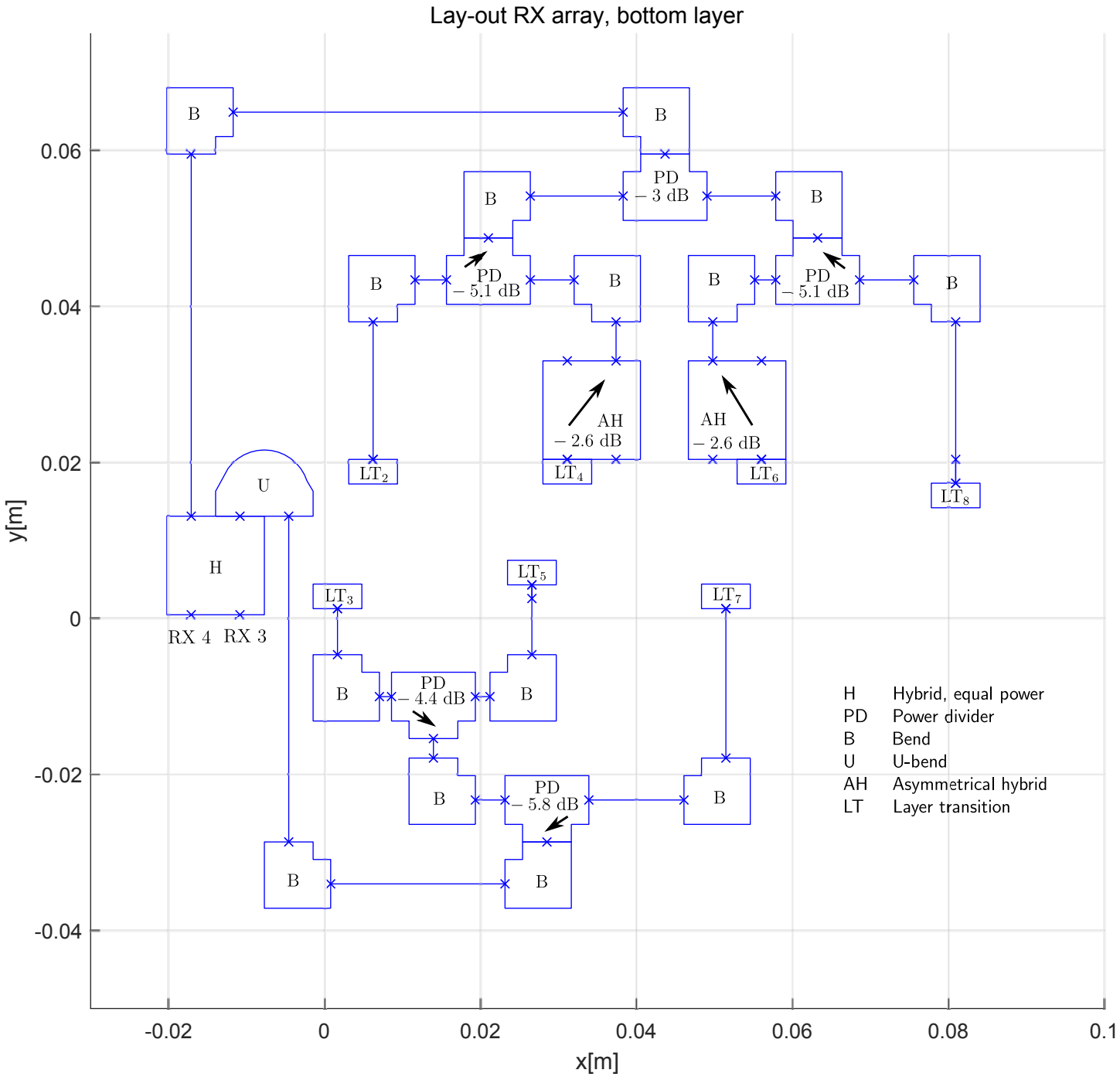

Figure 5.4: The precise component layout of the bottom layer of the receive array.

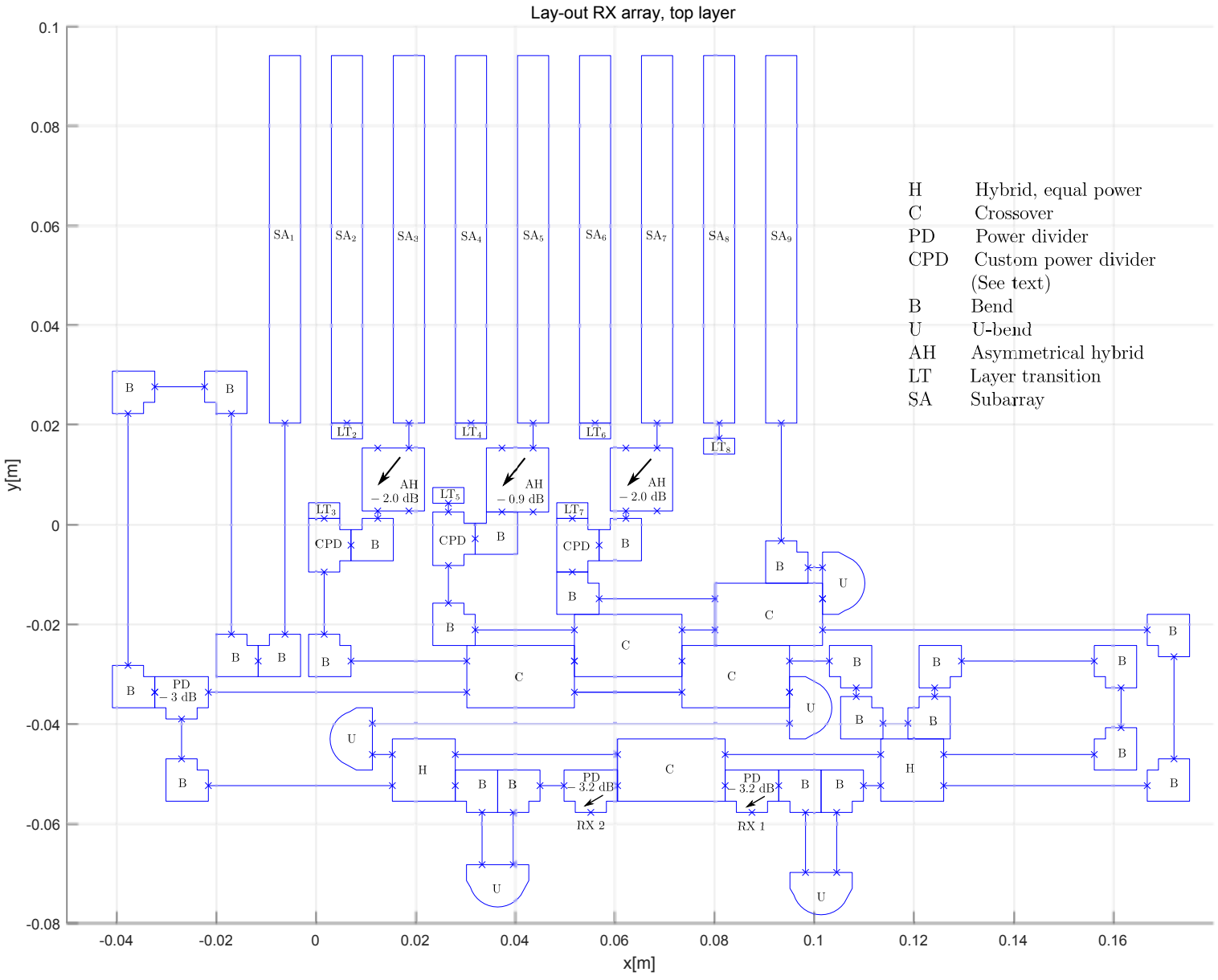

Figure 5.5: The precise component layout of the top layer of the receive array.

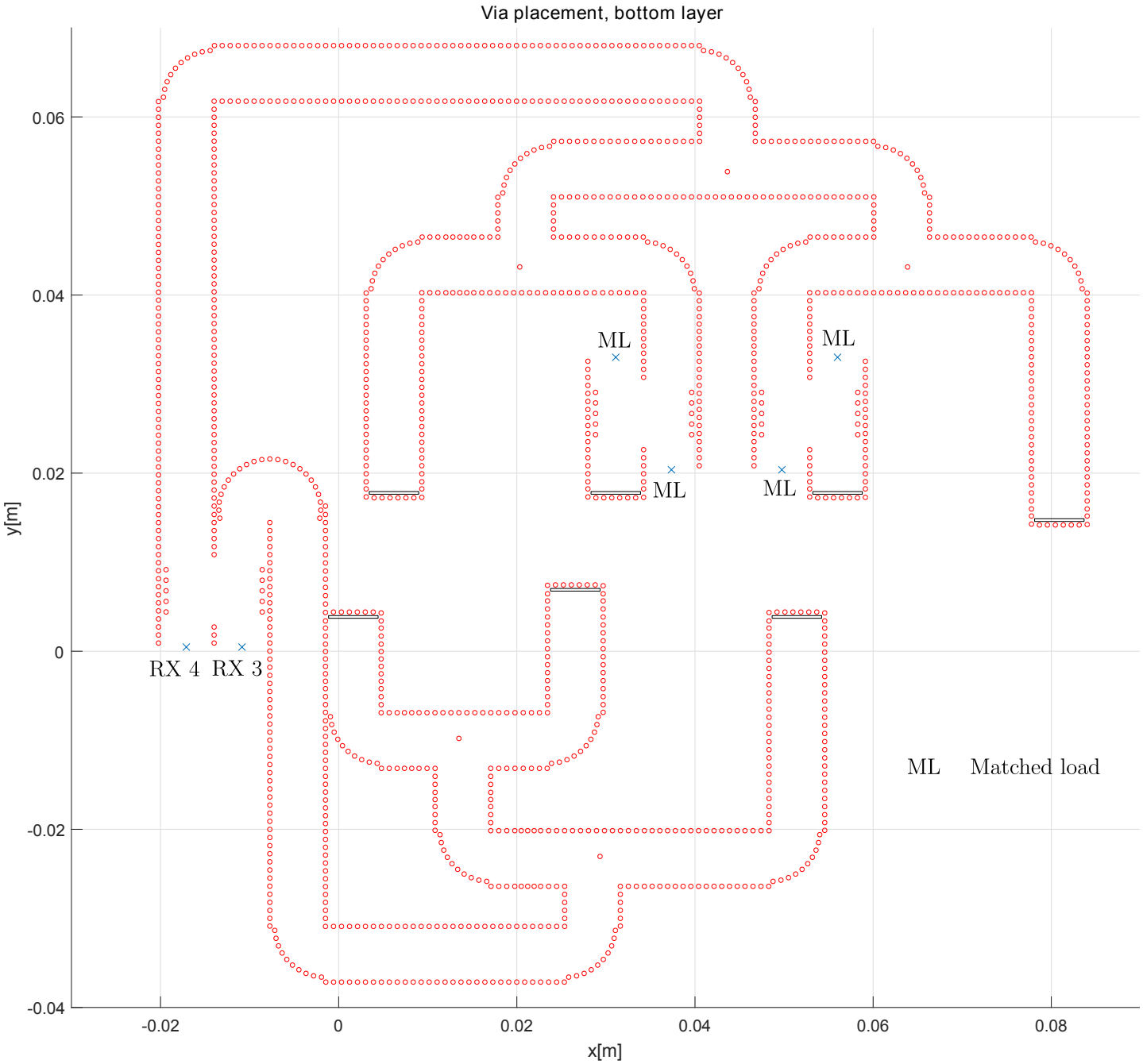

Figure 5.6: The implementation of the bottom layer of the receive array with vias.

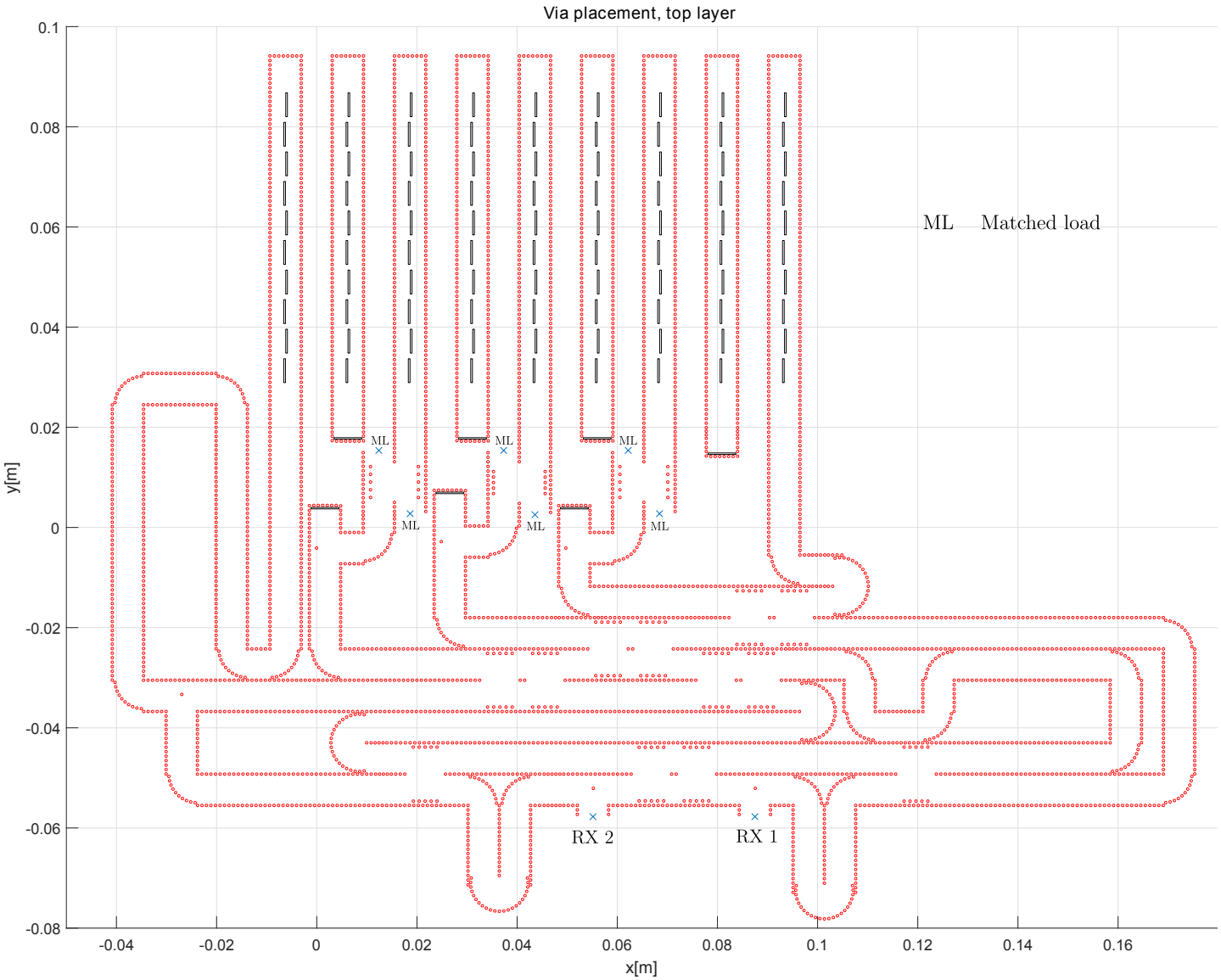

Figure 5.7: The implementation of the top layer of the receive array with vias.

5.3. CST simulation

The goal of this section is to show the CST model of the receive array, and to discuss the simulation results. Figure 5.8 shows the CST model of the bottom layer. There is a direct match with figure 5.6. Figure 5.9 shows the CST model of the top layer. There is a direct match with figure 5.7. Figure 5.10 shows the CST model of the full receive array, with bottom and top layer combined.

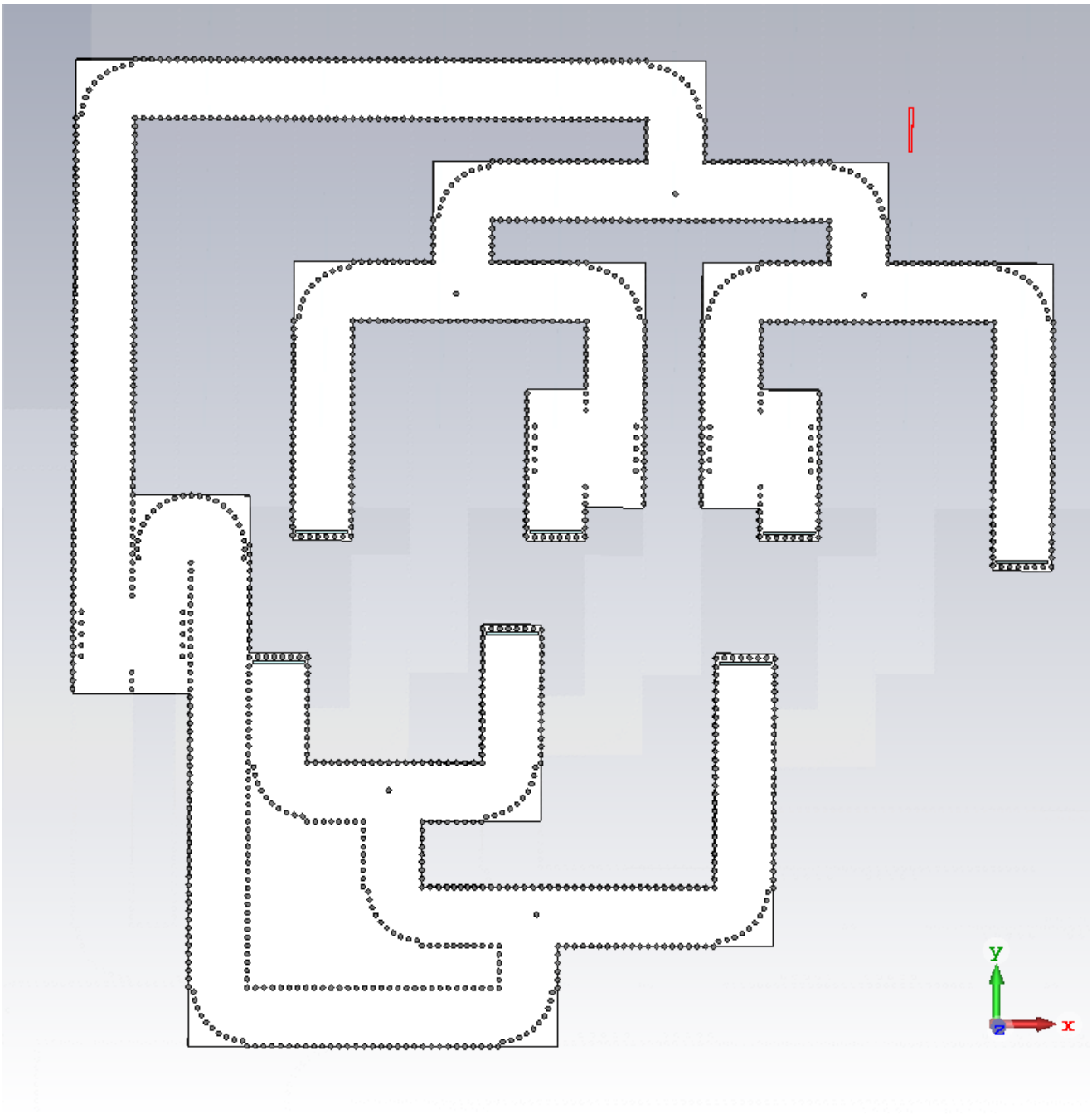

Figure 5.8: The CST model of the bottom layer of the receive array.

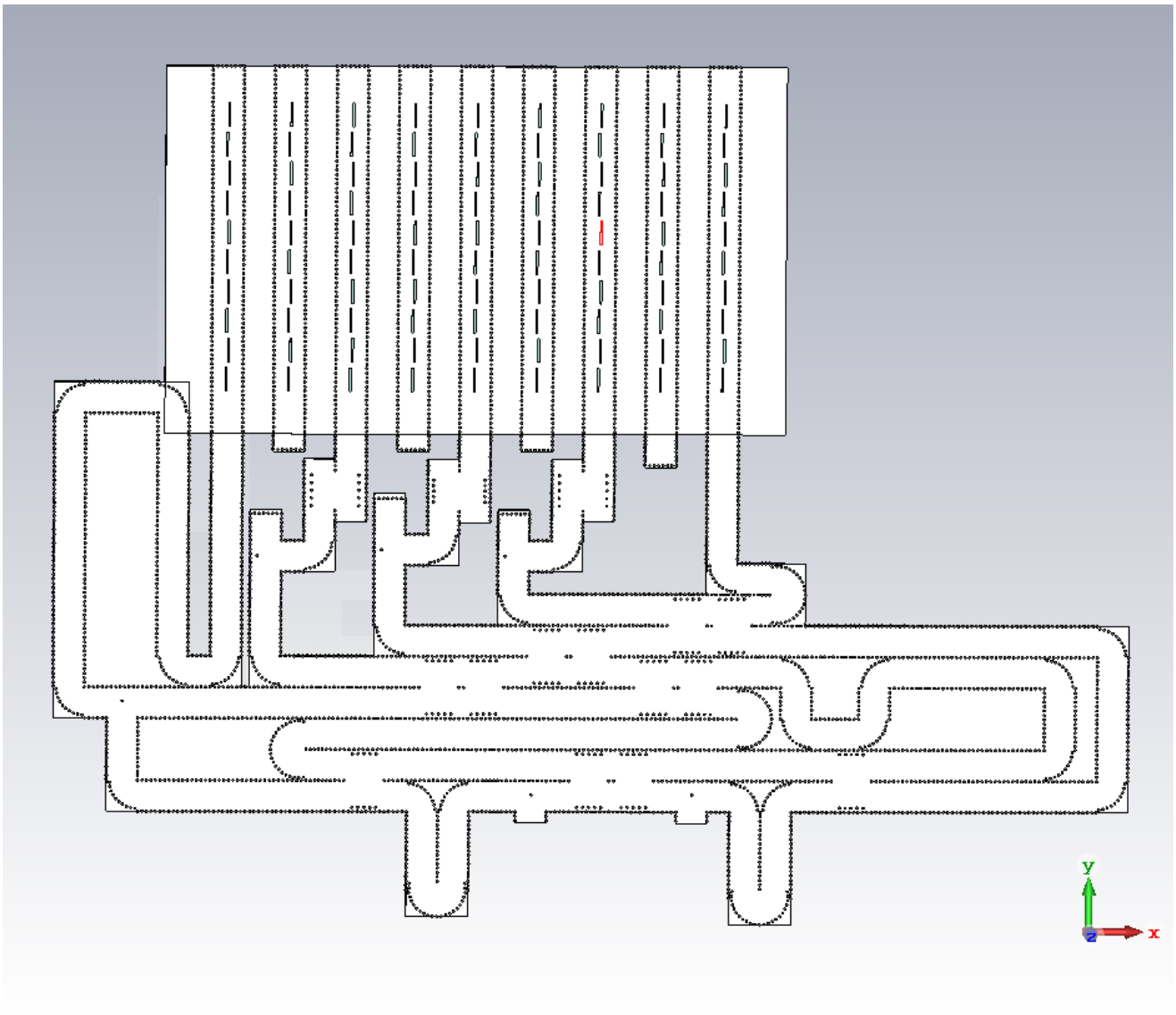

Figure 5.9: The CST model of the top layer of the receive array.

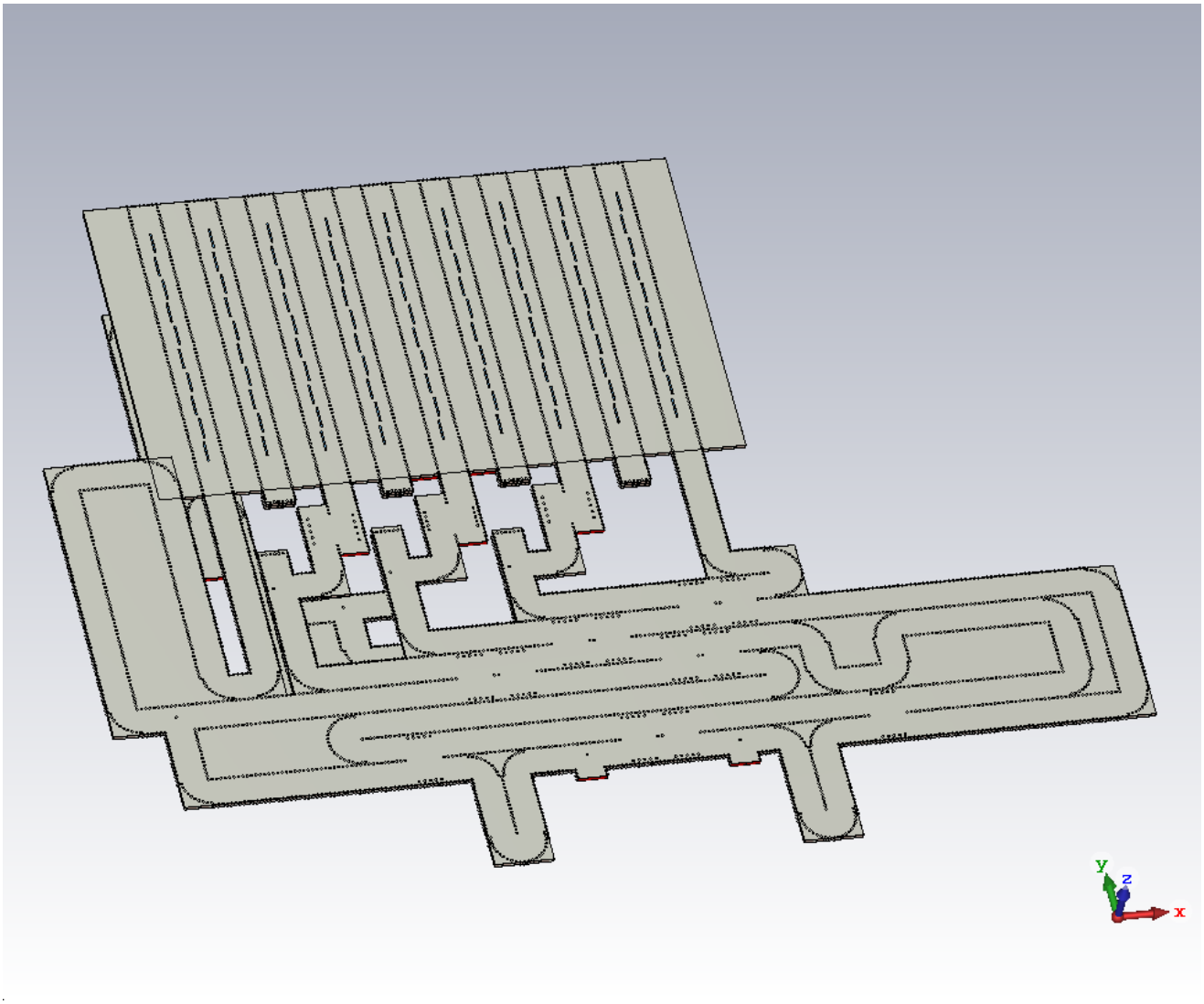

Figure 5.10: The full CST model of the receive array.

The full CST model was used to do simulations. First the beam patterns of the receive array were simulated. This is not as straightforward as for the transmit array. Since the receive array makes use of power attenuators, the receive array only functions properly when actually used in receive mode. However, for a CST simulation, it is more simple to simulate the beam pattern in transmit mode. Therefore, the simulated beam patterns were obtained as follows. First, the antenna subarrays were removed from the CST model. After this, the antenna beam coefficients were obtained by using the receive channels as input ports to the beamforming network. Next, the effect of the lossy networks was compensated using the designed values of the power attenuators. The coefficients obtained using this method were then fed to the subarrays. This method can introduce some error with respect to the full array, but should be good enough.
Figure 5.11 shows the simulated beam patterns. It can be seen that there is a good match with the desired beam patterns, that are created using the coefficients in table 5.1. For beam RX1 and RX2 the effect of mutual coupling is clearly visible. This effect was discussed before in 2, section 2.4. It can be seen that the grating lobe at broadside has a lower gain than the other grating lobes. The drop is 2.8 dB. The reason that the scan attenuation occurs at broadside is as follows. The antenna element spacing is 1λ. This means that the progressive phase shift that creates a beam at broadside, exactly matches the progressive phase shift of a beam in the endfire direction. The possibility for a beam in endfire direction increases the mismatch between the input of the antenna and free space.

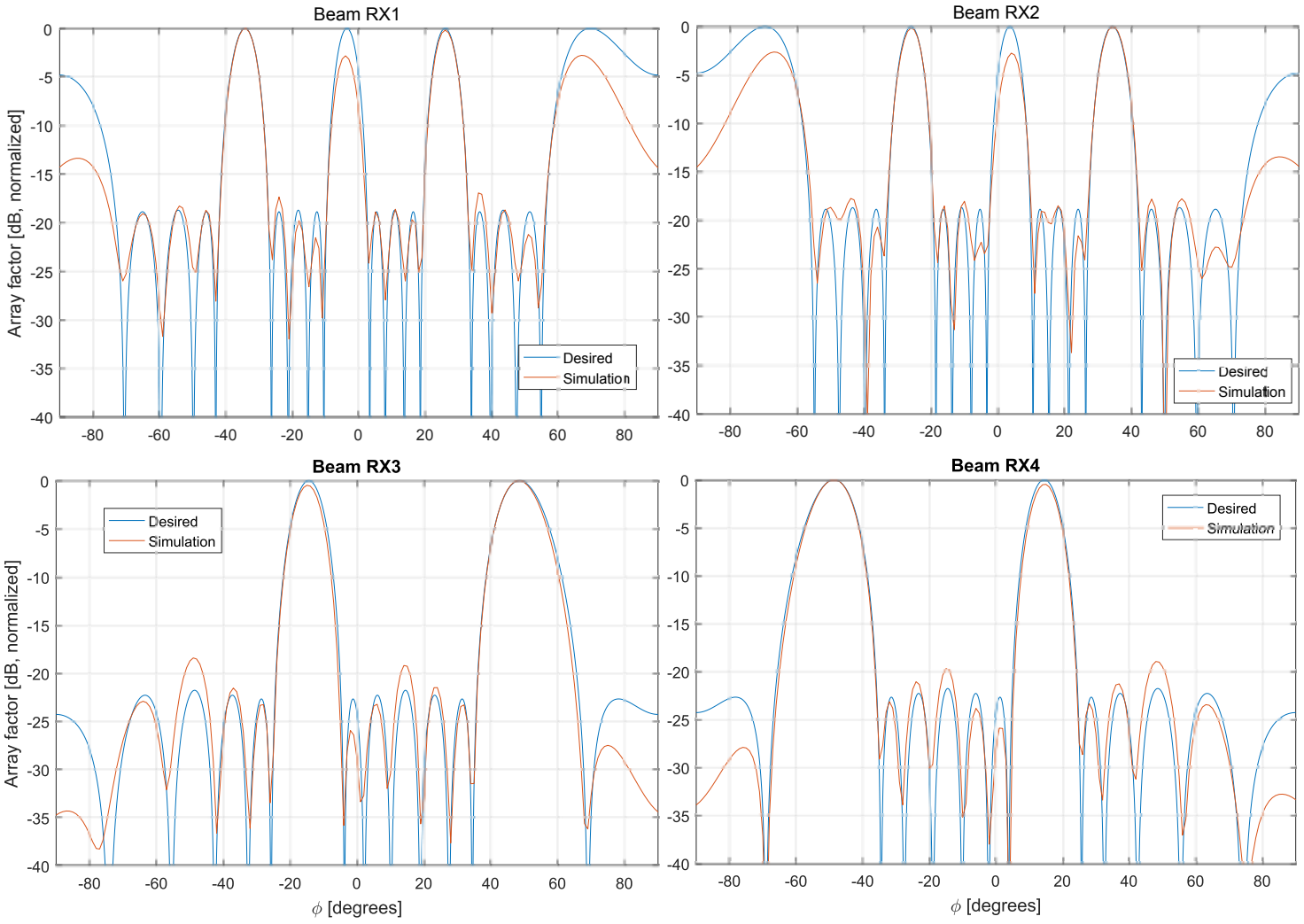

Figure 5.11: The receive beam patterns, that are simulated using the CST model.

To show the matching of the receive array, figure 5.12 shows the reflection coefficients the output channels. The top left figure show the reflection coefficients for port RX1. It can be seen that there is matching below -15 dB over a bandwidth of 0.7 GHz, which means that the bandwidth ratio is 3.1%. This does not

match the requirements, but the bandwidth is not very bad. The matching for port RX2 is similar. The bottom left figure shows the matching for channel RX3. It can be seen that there is an impedance match at the center frequency, but that it is only over a very narrow bandwidth. This is the case due to a design error. Without enough thought, part 1 and part 2 in figure 5.1 only combine correctly at a certain resonant frequency. For channel RX4 the result is similar. It is expected that ports RX1 and RX2 suffer from the same problem, but apparently this is to a lesser extent. Unfortunately, due to the design error, the receive array does not fulfill the bandwidth requirement. This does not affect the beam patterns at the center frequency. Therefore, the main concept can still be verified.

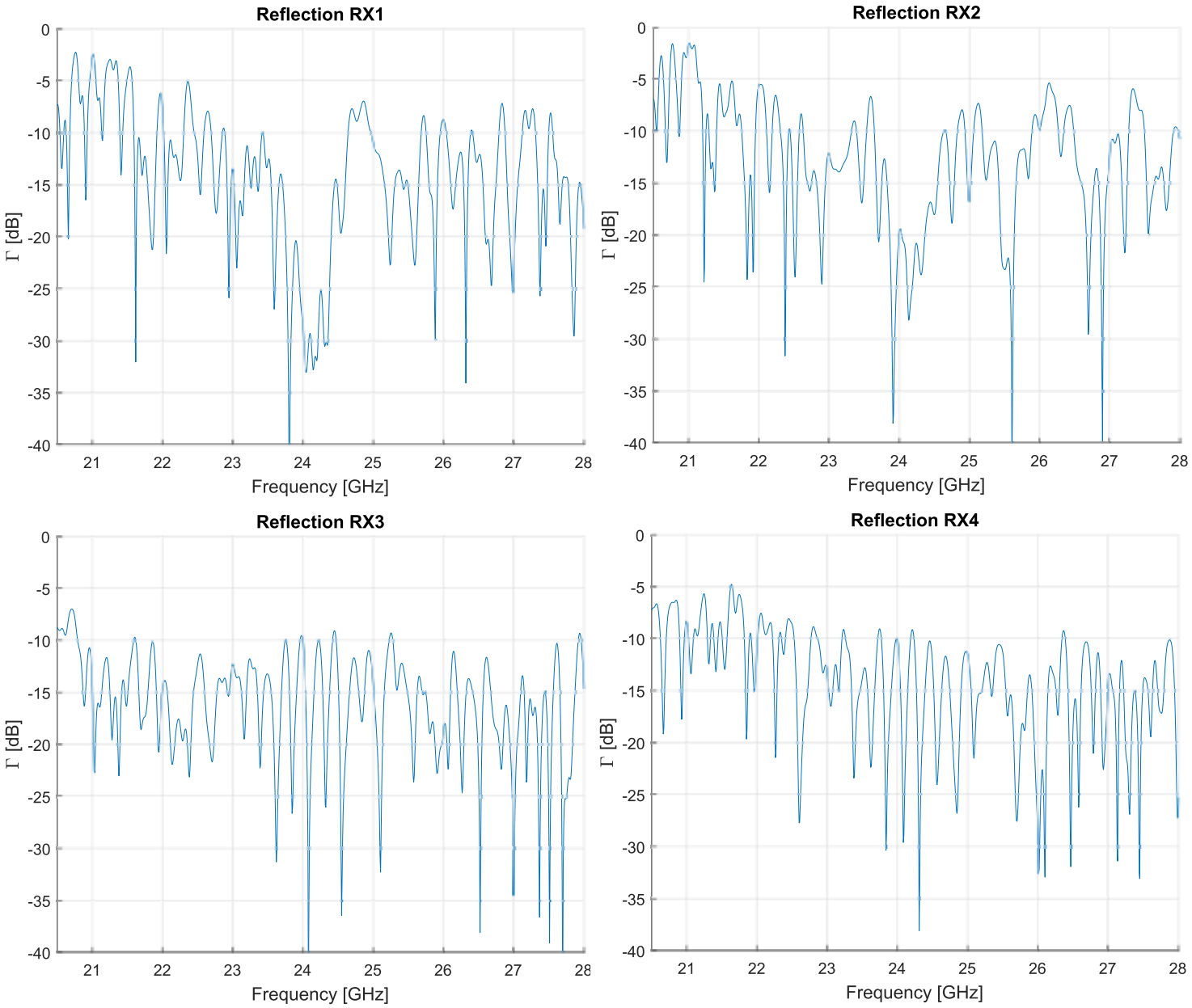

Figure 5.12: The reflection coefficients for all receive ports.

6

Combined arrays

The goal of this chapter is to show the beam patterns that are obtained, when the transmit and receive array are combined. Furthermore, the properties of the final design are summarized. In section 6.1 the simulated combined beam patterns are given. In section 6.2 the properties of the final design are summarized.

6.1. Combined beam patterns

The goal of this section is to show all combined beam patterns. The transmit array has been simulated, and the transmit beam patterns have been obtained. The same holds for the receive array. Now the simulated transmit beams and simulated receive beams are multiplied to obtain the total beam patterns. There are 3 transmit beams and 4 receive beams, so there will be 12 combined beam patterns.
Figure 6.1 shows all combined beam patterns, shown in seperate figures. In these figures, the desired combined beam patterns are also shown, first given in chapter 2, section 2.3. It can be seen that there is good match between the simulated beam patterns and the desired beam patterns. The SLL can become a bit higher due to the implementation, but in most cases, the deterioration is not too large. For all beams the sidelobe level stays below -15 dB, with the exception of beam TX1,RX4. In this case the SLL is -13.7 dB. Unfortunately, this would mean that requirement A1f for the sidelobe level is not achieved. However, the overall level of the sidelobes is still deemed quite acceptable. The average SLL for all 12 combined beams is -17.9 dB. It is important to note that in figure 6.1, all beams are normalized. This hides somewhat that the beams TX2, RX1 and TX2, RX2 suffer more from mutual coupling than the other combined beams. Therefore, this is repeated here.

Figure 6.2 shows all simulated combined beam patterns in a single figure. This figure may be compared with the desired case in figure 2.8. In figure 6.2, it can be seen that there is coverage from -50° to 50°. It can also be seen that some gaps occur between different beams. These gaps can be quite deep with respect to the peak power, but overall the performance is deemed to be acceptable. The peak gain in this figure does not match the actual gain of the total system.

6.2. Final design properties

The goal of this section is to summarize the properties of the final design. Table 6.1 shows the most important properties that are realized with the full CST system model. The half-power beamwidth that is given is at broadside. Both the average SLL performance and the worst-case SLL performance are given. The most important thing that can be seen from the table is as follows. The HPBW is very small, because the aperture is increased by using the grating lobe selection scheme. Furthermore, the SLL performance is also better than would be the case for uniform amplitude tapering. These advantages come at the cost of a reduced coverage.

Table 6.1: The properties of the final design.

Half-power beamwidth (HPBW)	5.7°
Aperture (TX and RX together)	9.5λ
SLL (Average 12 beams)	−17.9 dB
SLL (Worst of 12 beams)	−13.7 dB
Coverage	±50°

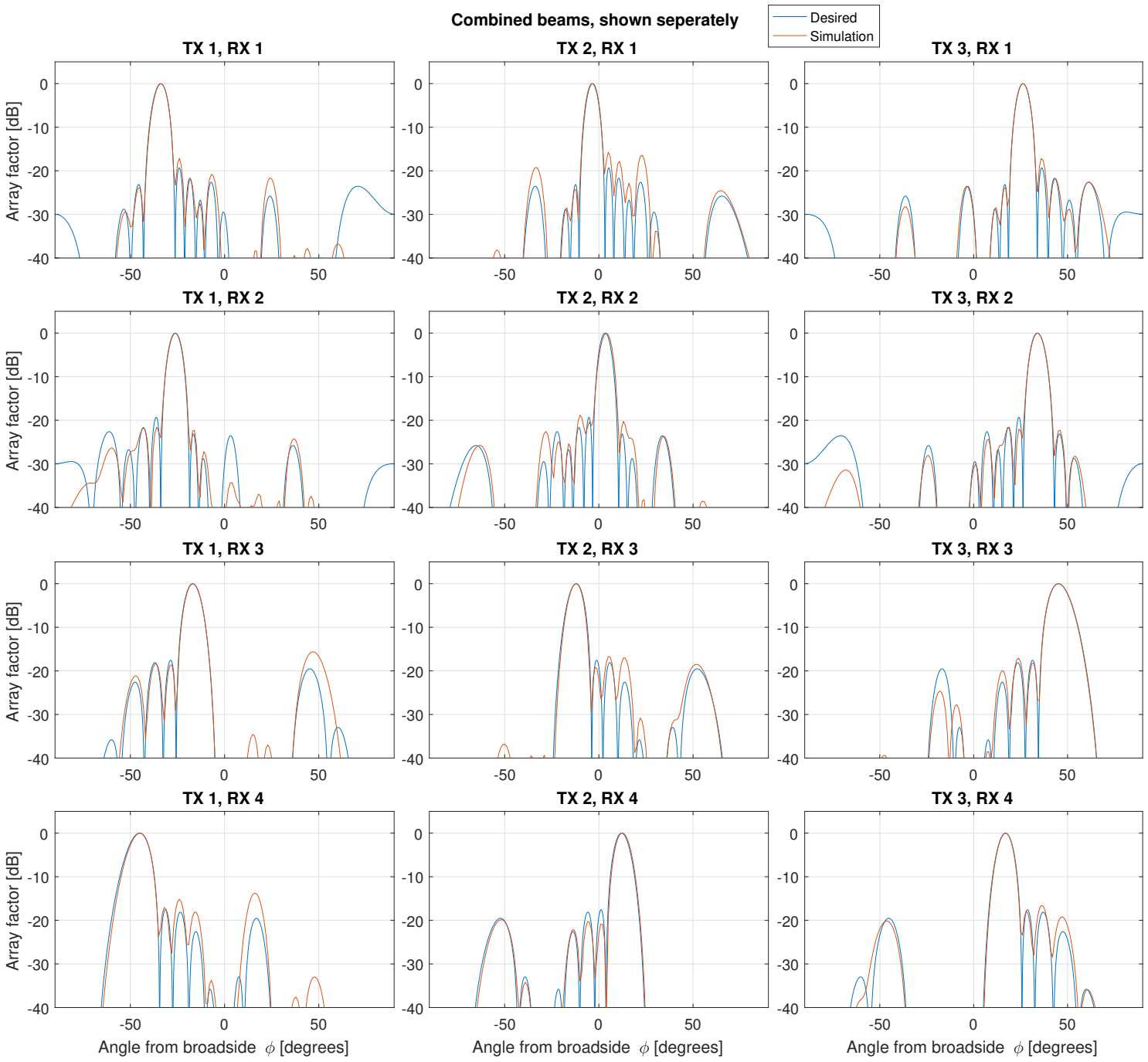

Figure 6.1: All the simulated combined beam patterns, shown seperately. It is important to note that beams TX2, RX1 and TX2, RX2 suffer more from mutual coupling than the other combined beam patterns. This is hidden somewhat, because all beams are normalized.

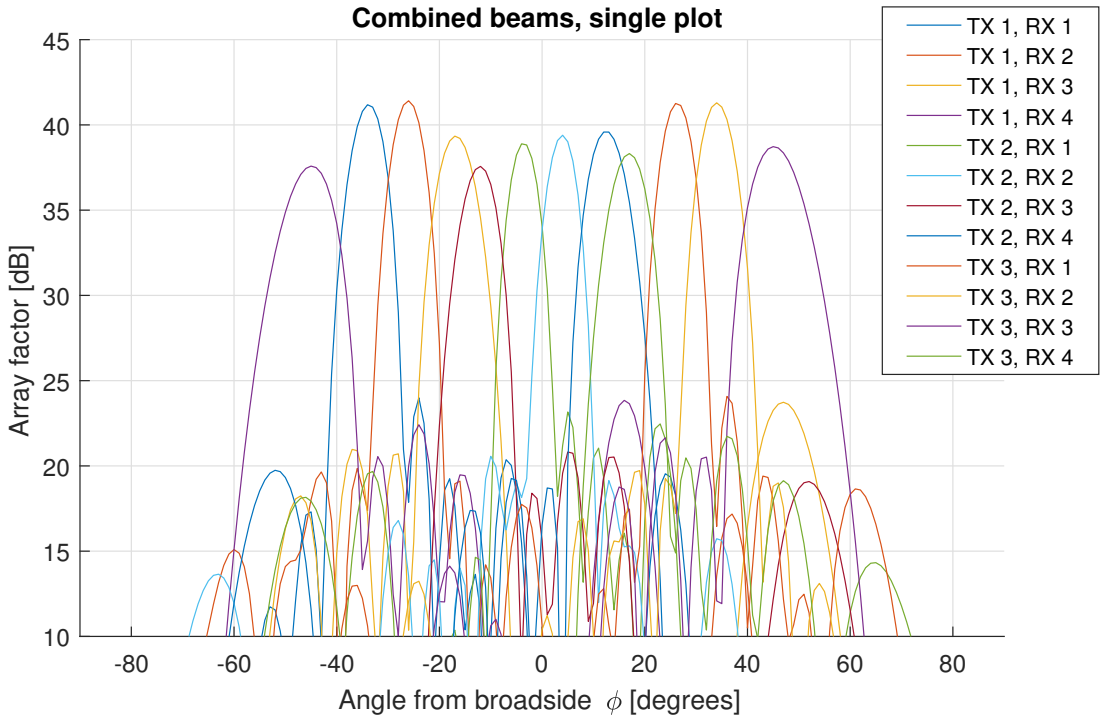

Figure 6.2: All the simulated combined beam patterns, shown in one figure.

7

Conclusions and future work

The goal of this chapter is to look back at the requirements for the system, to draw conclusions, and to determine what may be done in the future. In section 7.1 is discussed to what extent the requirements are fulfilled. In section 7.2 a conclusion of the thesis is given, and it is stated what was achieved in the thesis. Finally, in section 7.3 some recommendations for possible future work are given.

7.1. Fulfillment requirements

The goal of this section is to look back at the requirements in chapter 1, section 1.3, and to determine to what extent they have been fulfilled. This is done for the important requirements, and not for the requirements that are obvious or less relevant. Every requirement that is handled here will first be repeated shortly, and then will be determined whether it is fulfilled.

A1b This requirement was that the angular resolution in the azimuth direction should be better than for a state of the art MIMO implementation. In requirement A1b it was mentioned that for a state of the art system with 3 transmit channels and 4 receive channels, the HPBW at broadside is 8.4 to 9.5 degrees, depending on the SLL. The HPBW achieved in this thesis, with the same amount of channels, is 5.7 degrees, which is a significant improvement. This requirement is fulfilled.

A1c Requirement A1c stated that the final combined beam patterns should be able to provide unambiguous information. In figure 6.1 it can be seen that the combined beam patterns do not have grating lobes, so therefore this requirement is fulfilled.

A1d Requirement A1d stated that the gaps between adjacent beam options could be at most 8 dB lower than the peak power level. In figure 6.2 it can be seen that the largest gap is 9.3 dB lower than the peak power. Therefore this requirement is not fulfilled. However, these large gaps do not occur often, and the overall performance of the system is still more or less acceptable.

A1e Requirement A1e states that the coverage should be from azimuth angle $\phi = -45°$ to $\phi = 45°$. In figure 6.2 it can be seen that the achieved coverage is from $\phi = -50°$ to $\phi = 50°$. This requirement is fulfilled.

A1f Requirement A1f states that the SLL in the azimuth direction for all possible combined beams should be -15 dB. In figure 6.1 it can be seen that this does not hold for one of the twelve beam options. Therefore, the requirement is not fulfilled. However, for the other beams the SLL is good. Therefore, the overall system performance is still deemed to be acceptable.

A3a Requirement A3a gave the required bandwidth for the system. Unfortunately, by accident, a resonant structure was used in the receive array. This means that the final design is narrowband. This is the biggest design flaw, the requirement is not fulfilled. However, the concept of this thesis does not depend on the bandwidth, and can still be verified with this design.

B1a This requirement states that the scan attenuation due to mutual coupling may not be dominant. In figure 5.11 it can be seen that in the receiver, mutual coupling has an effect at broadside. The power drop is 2.8 dB, which is deemed acceptable. This requirement is fulfilled.

B2a This requirement states that the transmitter channels should be matched below -15 dB. This requirement is fulfilled.

B2c This requirement states that all receiver channels should be matched below -15 dB. Unfortunately this only holds for some of the receive channels, so this requirement is not fulfilled. However, for the channels that are not matched below -15 dB, the matching is still below -10 dB, so there is no total mismatch. The system can still operate.

B3e Requirement B3e states that the system should be scalable. For a system similar to the implementation in this thesis, it is possible to increase the amount of channels to some extent, without too much added complexity. However, this cannot be done too much, because the complexity would then become too high. To make a new system that can be used with a very large amount of channels, a new design is required. This requirement is partially fulfilled.

The fulfillment of the requirements can be summarized as follows. Some of the most important requirements are met, such as the requirement for the angular resolution in the azimuth direction, and the requirement for the angular coverage. Other requirements are not entirely fulfilled, but are not too far off. This is the case for the SLL, the matching of the channels and the gaps between combined beam patterns. The requirement that is not met at all, is the bandwidth, due to a design error. However, since the concept does not depend on the bandwidth, the design can still be used for verification. Overall, it can be said that the system is not perfect, but does perform reasonably well.

7.2. Conclusions

The goal of this section is to summarize what was done in the thesis, and to state what was achieved. The goal of this thesis was to implement a MIMO radar system, that provides improved angular resolution with respect to a state of the art MIMO radar. This was done as follows. A scheme was implemented that uses different transmit beam patterns, to select multiple grating lobes of the receive beam patterns. This is done in such a way, that full coverage of a reduced angular area is maintained. In this thesis, the scheme is called the grating lobe selection scheme. To implement it, beamforming networks are used on both the transmit- and receive side. To verify the concept, CST models of both the transmit- and receive array were created. The CST models were simulated, and there was a close match between the simulated beam patterns, and the desired beam patterns.
The following achievements were done in the thesis:

- **A MIMO radar design is provided that gives the possibility to improve the angular resolution, at the cost of a reduced field of view.** For many applications, it is not necessary to have a very wide field of view, and it is much more desirable to have a large angular resolution. Additionally, for many antennas, the element pattern does not even allow a large field of view. Therefore, it can be a waste of design resources, to have a system that has the ability to scan a large area. Again, the design in this thesis provides the possibility to fulfill this.
- **A scheme is provided, in which a limited amount of simple channels can still provide full coverage of some angular area.** In this thesis, every channel is directly coupled to a single beam pattern. The channels only need to have amplitude capabilities, no phase capabilities. This means that the complexity of the used digital chip can be reduced. No phase shifters are required. The concept gives the possible opportunity to reduce the cost of future radar systems.

It is believed this design provides a new approach for a MIMO radar system. More freedom in terms of performance and design complexity is created. Such freedom may be necessary to create future radar systems that have extreme performance.

7.3. Future work

In this section is discussed, what may be done to improve the design in the future, and to make the design more commercially viable. The following suggestions are done:

- **Improve the bandwidth.** In the current design, due to a thinking error, a resonating structure was used in the receiver, which means that the final solution is narrowband. For the radar to be more usable in the real world, a new design should be created that does not have this problem.

- **Remove the power attenuators.** In the current design, power attenuators are used to improve the antenna coefficients. It is not good to introduce losses, especially on the transmit side, where the power is high. It may be desirable to create a new design, that does not use attenuators.
- **Reduce the complexity of the analog beamforming networks.** Although the complexity of the digital chip may be reduced, because the channels no longer need phase capabilities, the analog beamforming networks that are used are quite complex. It may be desirable to create a new design, that uses beamforming networks with a lower complexity.

Bibliography

[1] J. Hasch, E. Topak, R. Schnabel, T. Zwick, R. Weigel, and C. Waldschmidt, "Millimeter-wave technology for automotive radar sensors in the 77 ghz frequency band," *IEEE Transactions on Microwave Theory and Techniques*, vol. 60, no. 3, pp. 845–860, 2012.

[2] B.-H. Ku, P. Schmalenberg, O. Inac, O. D. Gurbuz, J. S. Lee, K. Shiozaki, and G. M. Rebeiz, "A 77–81-ghz 16-element phased-array receiver with ±50° beam scanning for advanced automotive radars," *IEEE Transactions on Microwave Theory and Techniques*, vol. 62, no. 11, pp. 2823–2832, 2014.

[3] W. Menzel and A. Moebius, "Antenna concepts for millimeter-wave automotive radar sensors," *Proceedings of the IEEE*, vol. 100, no. 7, pp. 2372–2379, 2012.

[4] E. Fishler, A. Haimovich, R. Blum, D. Chizhik, L. Cimini, and R. Valenzuela, "Mimo radar: An idea whose time has come," in *Proceedings of the IEEE radar conference*, vol. 2004, pp. 71–78, Newark, NJ, USA, 2004.

[5] J. L. Butler, "Multiple beam antenna system employing multiple directional couplers in the leadin," June 7 1966. US Patent 3,255,450.

[6] A. Papadogiannis and A. G. Burr, "Multi-beam assisted mimo—a novel approach to fixed beamforming," in *2011 Future Network & Mobile Summit*, pp. 1–8, IEEE, 2011.

[7] M. Nedil, T. A. Denidni, and L. Talbi, "Novel butler matrix using cpw multilayer technology," *IEEE Transactions on Microwave Theory and Techniques*, vol. 54, no. 1, pp. 499–507, 2006.

[8] M. Bona, L. Manholm, J. Starski, and B. Svensson, "Low-loss compact butler matrix for a microstrip antenna," *IEEE Transactions on Microwave Theory and Techniques*, vol. 50, no. 9, pp. 2069–2075, 2002.

[9] S. Gruszczynski, K. Wincza, and K. Sachse, "Reduced sidelobe four-beam n-element antenna arrays fed by $4 \times n$ butler matrices," *IEEE Antennas and Wireless Propagation Letters*, vol. 5, pp. 430–434, 2006.

[10] R. Hansen, "Design trades for rotman lenses," *IEEE Transactions on antennas and propagation*, vol. 39, no. 4, pp. 464–472, 1991.

[11] K. Tekkouk, M. Ettorre, L. Le Coq, and R. Sauleau, "Multibeam siw slotted waveguide antenna system fed by a compact dual-layer rotman lens," *IEEE Transactions on Antennas and Propagation*, vol. 64, no. 2, pp. 504–514, 2015.

[12] D. M. Pozar, "The active element pattern," *IEEE Transactions on Antennas and Propagation*, vol. 42, no. 8, pp. 1176–1178, 1994.

[13] D. Pozar and D. Schaubert, "Scan blindness in infinite phased arrays of printed dipoles," *IEEE Transactions on Antennas and Propagation*, vol. 32, no. 6, pp. 602–610, 1984.

[14] S. Edelberg and A. Oliner, "Mutual coupling effects in large antenna arrays: Part 1–slot arrays," *IRE Transactions on Antennas and Propagation*, vol. 8, no. 3, pp. 286–297, 1960.

[15] H. Wheeler, "Simple relations derived fom a phased-array antenna made of an infinite current sheet," *IEEE Transactions on Antennas and Propagation*, vol. 13, no. 4, pp. 506–514, 1965.

[16] H. A. Wheeler, "The radiation resistance of an antenna in an infinite array or waveguide," *Proceedings of the IRE*, vol. 36, no. 4, pp. 478–487, 1948.

[17] H. Wheeler, "The grating-lobe series for the impedance variation in a planar phased-array antenna," *IEEE Transactions on Antennas and Propagation*, vol. 14, no. 6, pp. 707–714, 1966.

[18] M. Bozzi, A. Georgiadis, and K. Wu, "Review of substrate-integrated waveguide circuits and antennas," *IET Microwaves, Antennas & Propagation*, vol. 5, no. 8, pp. 909–920, 2011.

[19] J. Puskely, "Waveguide slot arrays." Presentation, TU Delft, 2018.

[20] F. Xu and K. Wu, "Guided-wave and leakage characteristics of substrate integrated waveguide," *IEEE Transactions on microwave theory and techniques*, vol. 53, no. 1, pp. 66–73, 2005.

[21] L. Yan, W. Hong, G. Hua, J. Chen, K. Wu, and T. J. Cui, "Simulation and experiment on siw slot array antennas," *IEEE Microwave and Wireless Components Letters*, vol. 14, no. 9, pp. 446–448, 2004.

[22] J. Hirokawa and M. Ando, "Single-layer feed waveguide consisting of posts for plane tem wave excitation in parallel plates," *IEEE Transactions on Antennas and Propagation*, vol. 46, no. 5, pp. 625–630, 1998.

[23] J.-H. Lee, T. Hirono, J. Hirokawa, and M. Ando, "A center-feed waveguide transverse slot linear array using a transverse-slot feed for blocking reduction," in *2008 IEEE Antennas and Propagation Society International Symposium*, pp. 1–4, IEEE, 2008.

[24] Y. Miura, J. Hirokawa, M. Ando, Y. Shibuya, and G. Yoshida, "Double-layer full-corporate-feed hollow-waveguide slot array antenna in the 60-ghz band," *IEEE Transactions on Antennas and Propagation*, vol. 59, no. 8, pp. 2844–2851, 2011.

[25] J. Xu, Z. N. Chen, and X. Qing, "Cpw center-fed single-layer siw slot antenna array for automotive radars," *IEEE Transactions on Antennas and Propagation*, vol. 62, no. 9, pp. 4528–4536, 2014.

[26] L. Nuria, "Course advanced electromagnetics." TU Delft, 2018/2019.

[27] S. Germain, D. Deslandes, and K. Wu, "Development of substrate integrated waveguide power dividers," in *CCECE 2003-Canadian Conference on Electrical and Computer Engineering. Toward a Caring and Humane Technology (Cat. No. 03CH37436)*, vol. 3, pp. 1921–1924, IEEE, 2003.

[28] Z. Hao, W. Hong, H. Li, H. Zhang, and K. Wu, "Multiway broadband substrate integrated waveguide (siw) power divider," in *2005 IEEE Antennas and Propagation Society International Symposium*, vol. 1, pp. 639–642, IEEE, 2005.

[29] A. Stevenson, "Theory of slots in rectangular wave-guides," *Journal of Applied Physics*, vol. 19, no. 1, pp. 24–38, 1948.

[30] A. Oliner, "The impedance properties of narrow radiating slots in the broad face of rectangular waveguide: Part i–theory," *IRE Transactions on Antennas and Propagation*, vol. 5, no. 1, pp. 4–11, 1957.

[31] R. S. Elliot, *Antenna theory and design*. John Wiley & Sons, 2006.

[32] G. Stern and R. Elliott, "Resonant length of longitudinal slots and validity of circuit representation: Theory and experiment," *IEEE Transactions on Antennas and Propagation*, vol. 33, no. 11, pp. 1264–1271, 1985.

[33] J.-W. Lian, Y.-L. Ban, C. Xiao, and Z.-F. Yu, "Compact substrate-integrated 4× 8 butler matrix with sidelobe suppression for millimeter-wave multibeam application," *IEEE Antennas and Wireless Propagation Letters*, vol. 17, no. 5, pp. 928–932, 2018.

[34] K. Wincza, A. Rydosz, I. Slomian, and S. Gruszczynski, "Reduced sidelobe multibeam antenna array with broadside beam fed by 4× 8 butler matrix," in *2015 International Symposium on Antennas and Propagation (ISAP)*, pp. 1–3, IEEE, 2015.